Chapter 7

Application of Non-destructive Testing for Measurement of Partial Discharges in Oil Insulation Systems

Tomasz Boczar, Andrzej Cichoń, Daria Wotzka,
Paweł Frącz, Michał Kozioł and Michał Kunicki

Additional information is available at the end of the chapter

http://dx.doi.org/10.5772/62409

Abstract

The subject area regards to metrology and measurement methods applied for non-destructive investigation of electrical discharges occurring in oil insulation systems of high-voltage devices. The main aim of performed research studies is a detailed and multivariate analysis of physical phenomena associated with generation of electrical partial discharges (PD), which occur in oil insulation of electrical equipment. An important cognitive component was the verification whether the form of PD has an effect on the energy contribution of the physical phenomena associated with their generation. For investigating the physical processes associated with generation of PD, a system for modelling, the study and analysis of physical phenomena associated with their generation in insulating oil were designed and implemented. In particular, the PD were simulated in three setups: (1) a surface system, (2) needle-needle system in insulating oil and (3) needle-needle system in insulating oil with gas bubbles. In these experimental setups, optical signals (IR, UV and visible), ultra–high frequency electromagnetic and high-energy X-ray radiation, acoustic emission and thermal images were registered. Recorded signals were subjected for multi-variant investigation and analyses in the time and frequency domains. The contribution of particular physical phenomena was determined.

Keywords: partial discharge, non-destructive testing, signal processing and analysis, paper-oil insulation, power transformer, diagnosis, non-conventional diagnosis of PD

1. Introduction

The generation and development of partial discharges (PD) in solid, liquid and gas dielectrics associate numerous physical phenomena. The most important are occurrence of a current pulse, emission of electromagnetic waves of ultra–high frequency (UHF), generation of optical radiation and high-energy radiation (X-/gamma rays), chemical transformations in the isolation, an elastic shock deformation and the associated acoustic wave generation. Based on these phenomena, diagnostic methods have been developed for detection, measurement and localization of PD, which may occur in insulating systems of power devices [1–8]. Currently, the assessment of electrical discharges shall apply the following non-destructive methods: electric [9–13], gas chromatography and acoustic emission (AE) [14–20] as well as the optical method [21–23]. Measurements are also performed as approximation of the amount of emitted heat, light and pressure changes in the PD generation area. It should be noted that each method has its advantages and limitations in application. In the normal operation of power devices, PD measurement by the electrical method is due to high levels of electromagnetic interference practically impossible. In the method of gas chromatography, serious problem is regarding the possibility of falsifying the test results while getting and transporting the insulating oil samples. Whereas, in the EA method there are problems associated with the localization of PD generation area location. At the same time, the information obtained through the application of these methods is a direct reason for their intensive development and improvement. Works carried out so far for the estimation of their applicability in the diagnosis of insulation systems of power devices have focused mainly on issues related to the selection and improvement of the measuring apparatus. They also concerned improvement of the recording methods, the analysis and interpretation of measurement results obtained mainly within modern signal processing algorithms and specialized computer software applied in this field. High-power transformer diagnostics that is based on PD measurement issues a problem of selection of indicators that would enable for correlation of measurements results with particular defects types, which are the source of discharges. These indicators should properly characterize the phenomena of formation and development of PD in insulating systems. Therefore, it appeared necessary to execute experimental studies aimed in understanding the physical processes associated with the generation of PD and thus enabling the evaluation of the energy contribution of individual phenomena using signal processing methods. In consequence, the results obtained with different testing methods enabled for linking and identification of the dominant processes whose measurement is essential for a proper evaluation of the measured isolation. Implementation of such analyses should help to reduce the risk of errors in the diagnosed isolation evaluation, which in turn can have a direct impact on economic and financial dimension.

The main cognitive objective of the research works was a detailed and multi-variant study of the physical phenomena associated with formation and development of electrical PD generated in liquid dielectrics. PD were measured with the following methods: acoustic, electric, gas chromatography, optical spectroscopy. The following research hypothesis was set up in the research: it is possible to experimentally investigate the physical processes associated with generation of the fundamental forms of PD that may occur in insulating oil and their reciprocal relation. This applies particularly to the development of a relationship and contribution of

http://dx.doi.org/10.5772/62409

various forms of radiated energy. Consequently, it allowed identifying those physical phenomena, associated with the formation of PD, which are dominant in terms of energy and thus have the greatest impact on the development of aging processes in the studied isolation. An important cognitive element was estimation of whether the form of a PD affects the energy contribution of the physical phenomena associated with their generation.

The results obtained may be applied for monitoring and comprehensive evaluation of the considered isolation. Inclusion during the tests performed on-line, all of the results obtained by different methods may increase the confidence of inference about the technical condition of the insulation equipment, and thus it may contribute to increase their work reliability, extend their operation time and avoid unexpected failures, which in turn can bring measurable economic benefits. This applies in particular to large power transformers, in which investment cost in relation to the total value of equipment used for transmission, distribution and distribution of electricity represents about 20%. Moreover, the expected cost of transformer failure in extreme cases can exceed up to five times its purchase price, while the total costs of the non-invasive diagnostic measurements of transformer insulation systems do not exceed 10% of its repairs cost. The above-mentioned findings justify the broad diagnostic procedures conducted within the research, the scope of which is correlated with the technical and economic importance of the measured electric power equipment.

2. The experimental part

To investigate the physical phenomena associated with generation of PD, a research station allowing for simulation and studying the phenomena of PD generation in insulating oil was designed and practically implemented. Also, the spark gaps for modelling of PD in surface (SURF), needle-needle (NN) and needle-needle with gas (air) bubbles (NNB) systems were designed and manufactured. The multi-variate experimental studies, performed under laboratory conditions, consisted of simultaneous recording of acoustic emission, electrical and optical signals, electromagnetic radiation of ultra–high frequency and high-energy X-, alpha, beta and gamma rays, which were generated by three considered fundamental forms of PD. The mentioned methods were applied during all planned trails. The trails included PD generation at different supply voltage levels, starting from 0 V and finishing by the breakdown voltage, which was different in the sub-sequential trials.

A professional test apparatus which enables measurement and analysis of acoustic emission (AE) signals was applied: PULSE DynXI system type 3050-B-A4 from Bruel&Kjael, numerical measuring instrument type 945A from SVAN, instrumentation transducers 4514-B-001 100mV/g and 4513-B-002 500mV/g, amplifiers with the power suppliers type Nexus from Bruel&Kjael, instrumentation cards Acquitec CH-3160, instrumentation computer Dell E6400 ATG, instrumentation computer Atlas ATXB-150. The AE signals were recorded for each type of PD modelling setup and for various levels of the supply voltage. Results of studies related to the AE are depicted in Section 3.3.

In order to implement the proposed research works connected with measurement and analysis of optical radiation generated by the modelled basic forms of PD, a spectrometer, HR4000 from Ocean Optics, equipped with multi-grating which allows for analysis of optical radiation spectra in the range from at least 270 to 1700 nm with a resolution of about 0.5 nm, was applied. The recorded signal is supplied to the grid by optical fibre. The sensor can be immersed in the insulating oil, which enabled measurements in the very vicinity of the PD generation location. The studies included measurement trails conducted at various distances of the sensor to the PD generation area. Results of studies related to the spectrophotometry are depicted in Section 3.2.

Also, a professional UVollé camera from OFIL, which enables registration of PD in the ultraviolet spectrum (in the range from 250 to 280 nm) and visible region, was applied. This camera can not be immersed in oil, thus UV measurements were performed at larger distances to the PD generation area, outside of the tank, where the electrodes were mounted. The analysis of results depicted no UV radiation outside of the tank; thus, this analysis is not included in this chapter.

Furthermore, the equipment included a PDS 100 device from Double that allows for measurements of the electromagnetic disturbances levels in the range from 50 MHz to 1 GHz. Additional measurement and research apparatus include: a multi-channel PD measurement and detection system with the electrical method, equipped with PD detectors, an external module for interferences elimination, UHF probe and software to analyze and evaluate the measuring results, according to the requirements of IEC 60270–2000 standard. Results of studies related to the electrical and UHF methods are depicted in Section 3.1.

Another instrument, which was partly built and partly purchased, is a setup for study of high-energy radiation comprising X-, gamma, alpha and beta ray sensors and equipment for acquisition of pulses representing the measured value of radiation (counters). Similar as it was the case of UV camera, the high-energy radiation sensor was mounted near the oil surface, at a larger distance to the PD generation area. The analysis of results depicted no high-energy radiation outside of the tank, thus this analysis is not included in this chapter. If interested, the reader is referred to [24,25], where the authors present results of PD high-energy radiation measurements in a gas-insulated system.

During an 8-hour period of time, the emitted infrared radiations were registered using an infrared camera, type ThermoGear G100EX, from NEC that allows for registration of electromagnetic radiation in the range from 8 to 13 microns, which is in the mid-infrared (MIR) frequency band (typically 5–30 microns). The camera is equipped with NS9500Lite software that is used to analyze the thermal images. Results of studies related to the infrared technology are depicted in Section 3.4.

The measuring setup along with the applied instrumentation and chosen preliminary results of the considered research were described in detail in [26], thus its presentation was omitted in this chapter. For archiving and processing of the measured data, numerical procedures implemented in the Matlab programming environment were applied.

http://dx.doi.org/10.5772/62409

The physical and chemical properties of applied insulation oil were investigated by means of a chromatographic analysis of collected oil samples, which was conducted by a specialist chemical laboratory. Results of studies related to chromatography are depicted in Section 3.5.

3. Analysis of measurement results

All gathered signals were subjected to a comprehensive processing and analysis. In the following sections, the achieved results are given. The particular measurement methods are juxtaposed for the three measuring setups for better comparison.

3.1. Results of analysis obtained using the electrical and UHF methods

The first step in the analysis of data gathered with the electrical and UHF method was to consider the background environment. **Figure 1** depicts the spectrum of UHF sweep, at which there were no significant interferences detected. In **Figures 2–4** the UHF amplitude spectra for PD measured in the needle-needle system with air bubbles, the needle-needle system and the surface system are depicted, respectively. Based on these spectra, three frequencies for each setup were selected, at which the UHF measurements were performed:

- For the NN system: 350, 480, 580 MHz
- For the NNB system: 350, 460, 560 MHz
- For the SURF system: 390, 485, 570 MHz

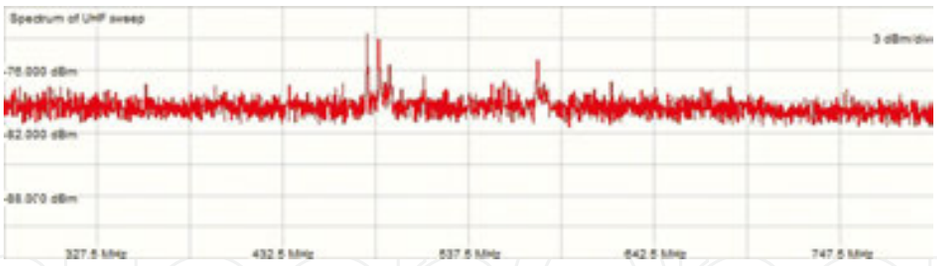

Figure 1. The UHF amplitude spectrum for background noise.

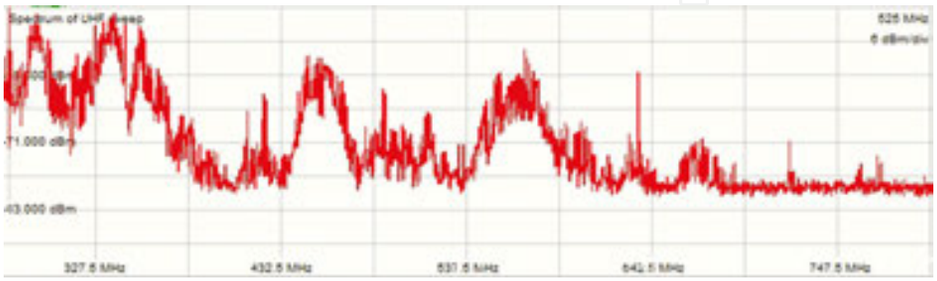

Figure 2. The UHF amplitude spectrum for PD measured in the needle-needle system with air bubbles.

Figure 3. The UHF amplitude spectrum for PD measured in the needle-needle system.

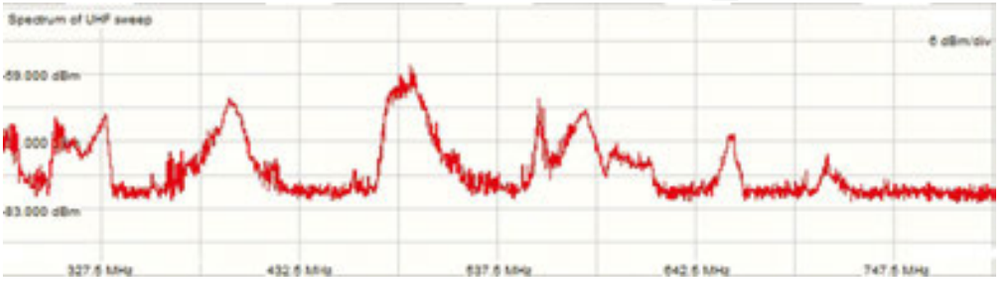

Figure 4. The UHF amplitude spectrum for PD measured in the surface system.

The gathered charges, measured with the electrical method and voltages, measured with the UHF method were subjected to further analysis. The collected data were depicted in the form of histograms, illustrating the relation of the apparent charge and voltage values, in the function of time that was registered during 1 min for each trail. An example is depicted in **Figure 5**.

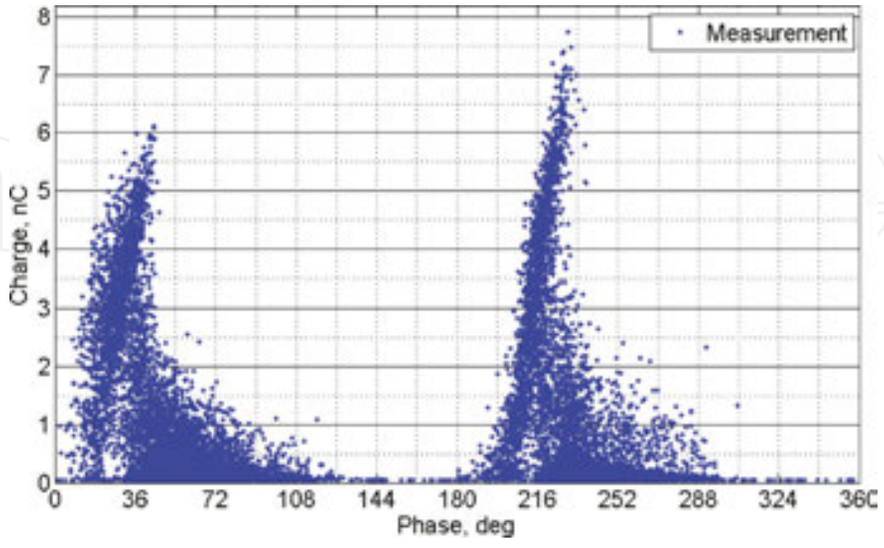

Figure 5. Charge values measured with the electrical method at the frequency f = 480 MHz, during the generation of PD at supply voltage U = 29 kV in the NN system.

http://dx.doi.org/10.5772/62409

For each phase of the supply voltage, the maximal intensity was chosen. The resulted curve was subjected for an interpolation using local regression and weighted linear least squares with a second-degree polynomial model. An example is depicted in **Figure 6**.

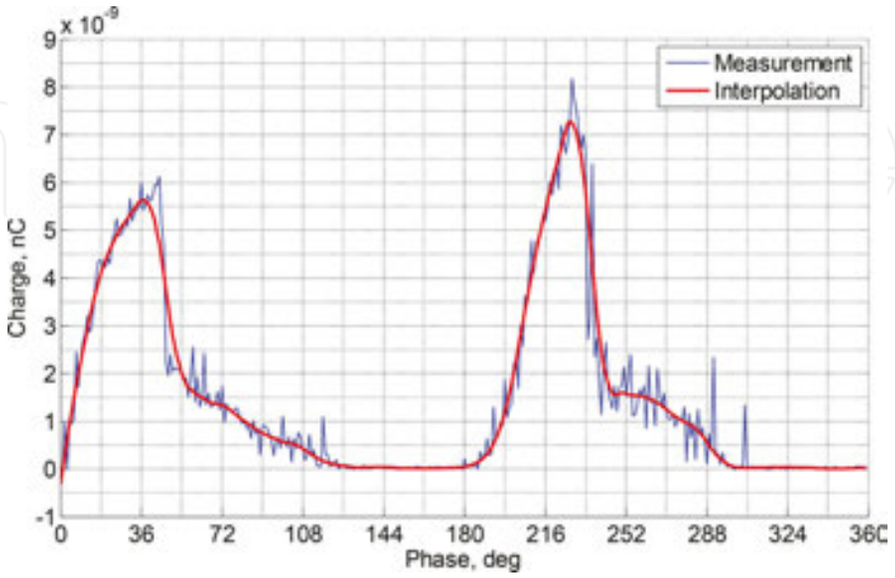

Figure 6. Envelope over the maximal charge intensities and its interpolation as the function of phase. Data measured for f = 480 MHz, U = 29 kV in the NN system.

The mentioned procedure was conducted for all measured signals. For better comparison for each of the considered PD type and generation voltage, the particular interpolates were plotted in one chart. An example is depicted in **Figure 7**.

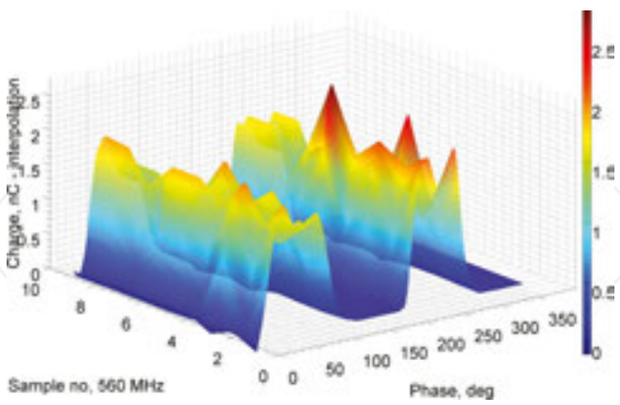

Figure 7. Interpolates over 10 measurements performed with the electrical method for f = 560 MHz, U = 56 kV in the NNB system.

The gathered interpolates for same PD type and generation voltage were averaged. The achieved arithmetical means were plotted into one chart to observe the influence of the PD generation voltage on the registered data. In **Figures 8–13**, the dependencies for the charge values and voltage values measured in the NN system are presented.

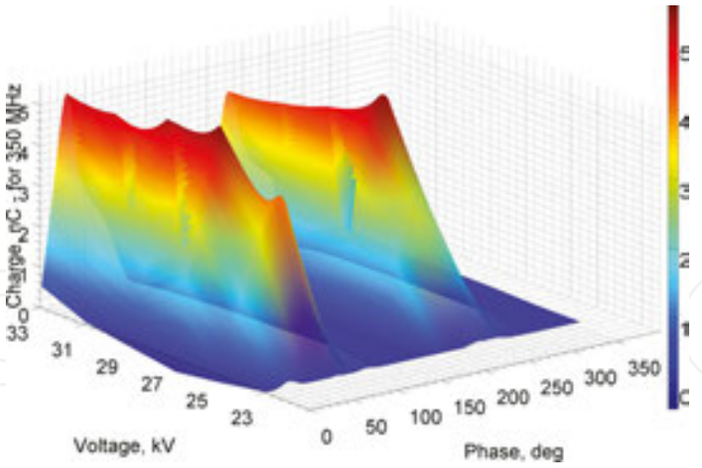

Figure 8. Charges measured at f = 350 MHz.

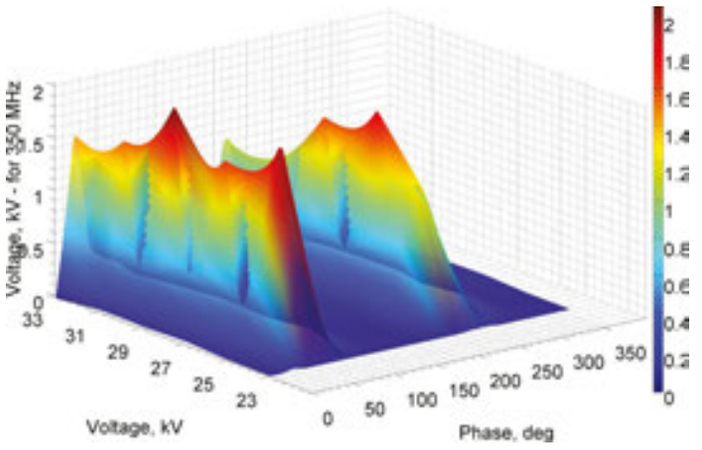

Figure 9. Voltages measured at f = 350 MHz.

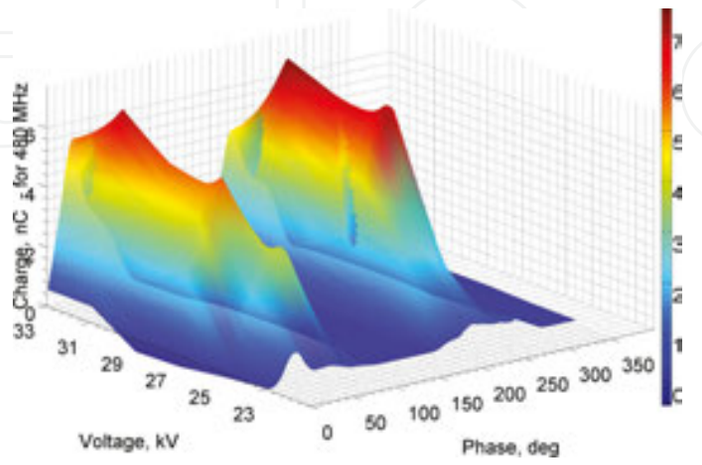

Figure 10. Charges measured at f = 480 MHz.

http://dx.doi.org/10.5772/62409

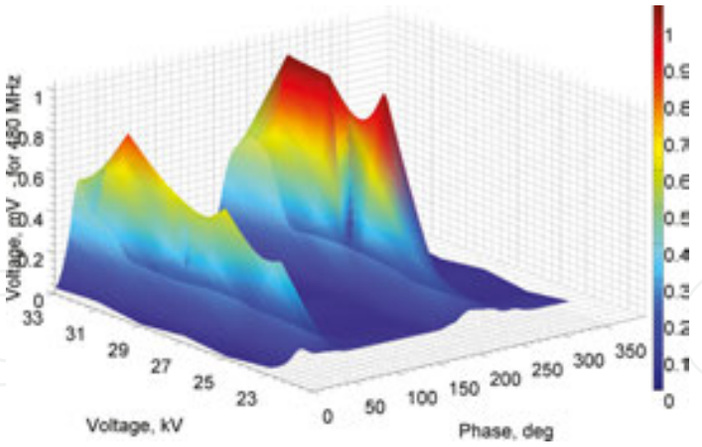

Figure 11. Voltages measured at f = 480 MHz.

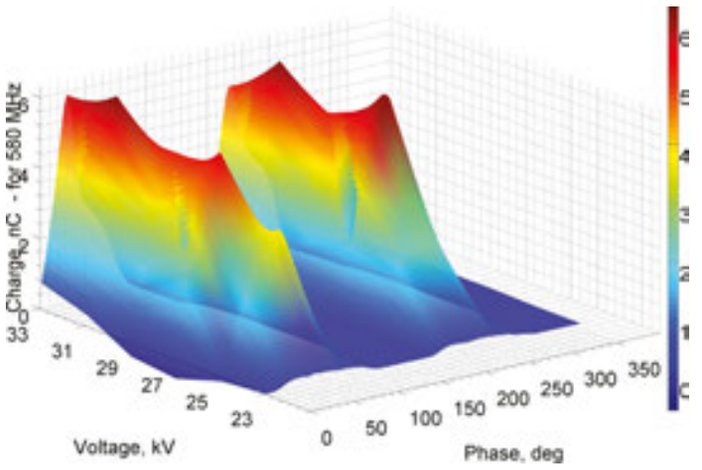

Figure 12. Charges measured at f = 580 MHz.

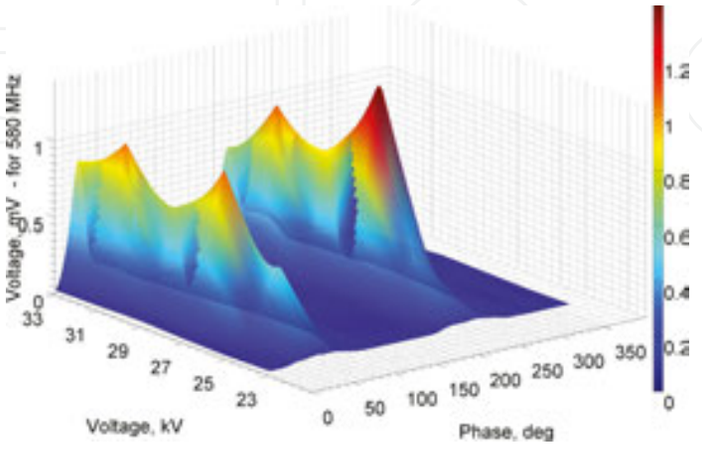

Figure 13. Voltages measured at f = 580 MHz.

In **Figures 14–19**, the arithmetical means over the interpolates in the function of phase and PD generation voltage, measured in the SURF system, are presented.

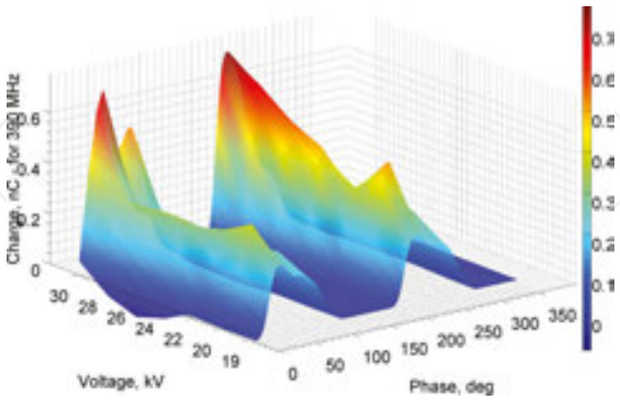

Figure 14. Charges measured at f = 390 MHz.

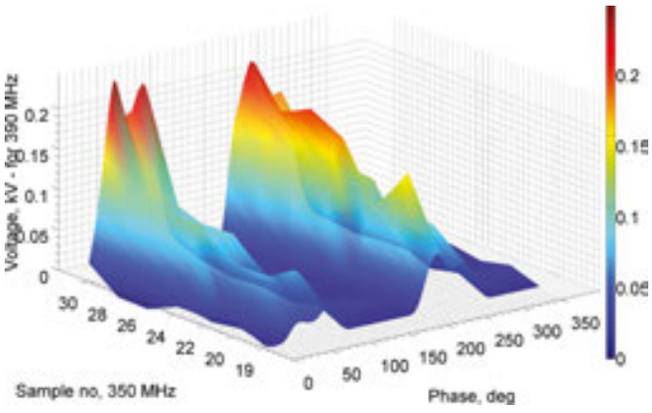

Figure 15. Voltages measured at f = 390 MHz.

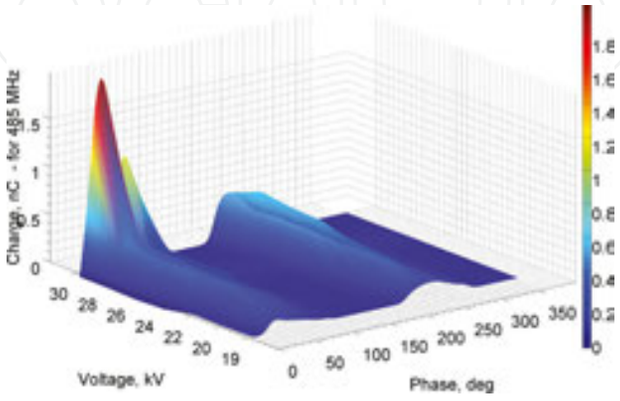

Figure 16. Charges measured at f = 485 MHz.

http://dx.doi.org/10.5772/62409

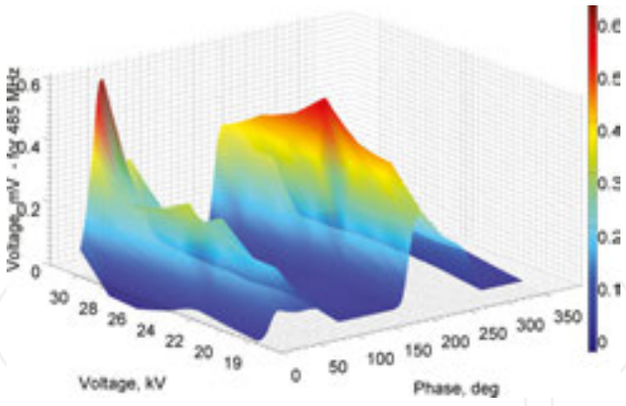

Figure 17. Voltages measured at $f = 485$ MHz.

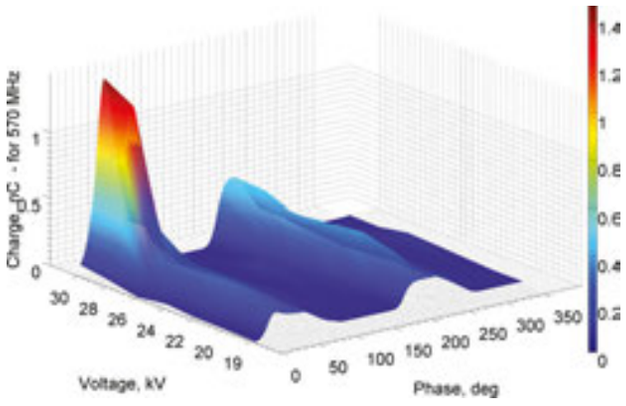

Figure 18. Charges measured at $f = 570$ MHz.

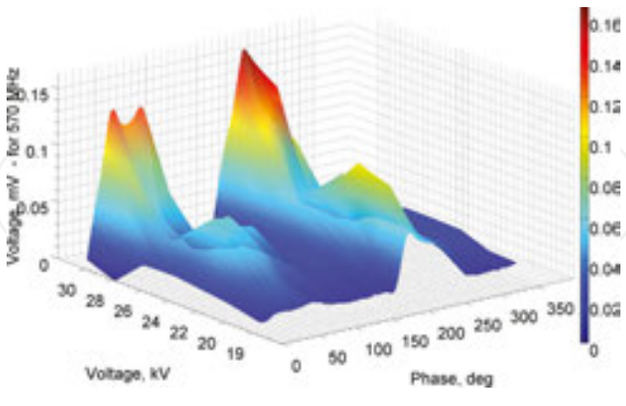

Figure 19. Voltages measured at $f = 570$ MHz.

The next type of analysis considered calculation of the empirical distribution (histograms) of the registered data for each of the phase of the PD generation voltage. In **Figures 20–25**, the results for charges and voltages registered at the selected frequencies, while generating PD at $U = 30$kV in the SURF system, are presented. In the case of charges, registered with the electrical

method, there are no significant differences between the three considered frequency ranges to recognize. In the case of voltages, registered with the UHF method, the densities are different for the particular frequency ranges.

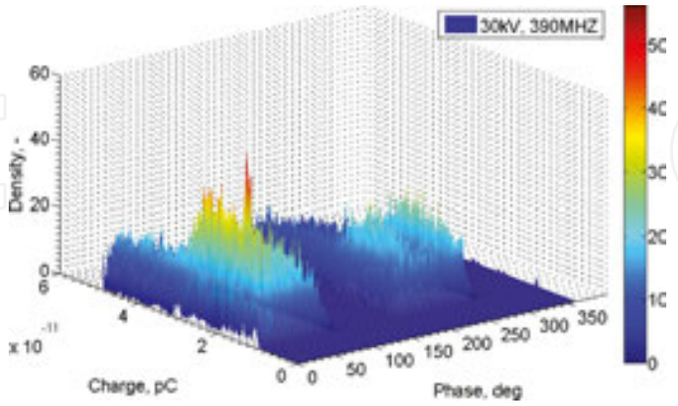

Figure 20. Charges measured at f = 390 MHz.

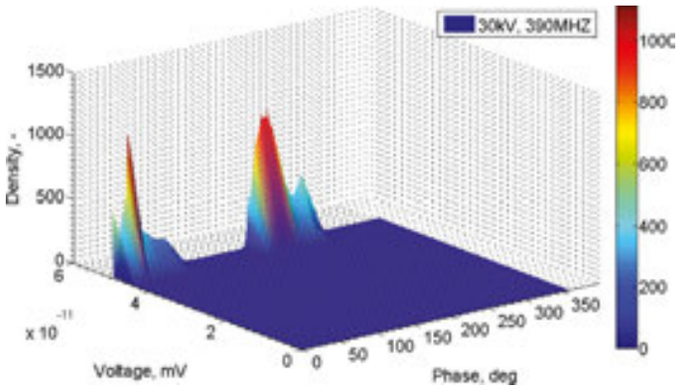

Figure 21. Voltages measured at f = 390 MHz.

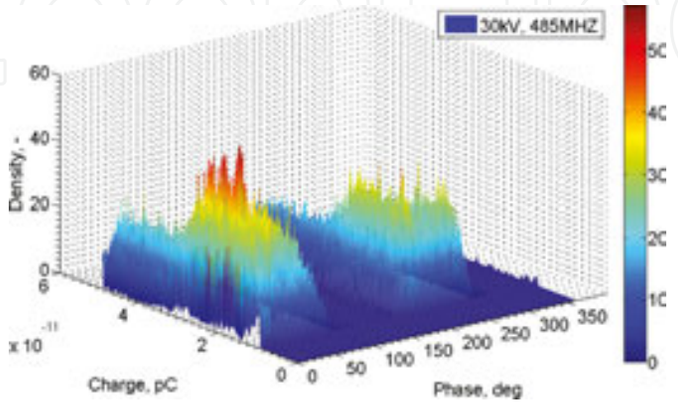

Figure 22. Charges measured at f = 485 MHz.

http://dx.doi.org/10.5772/62409

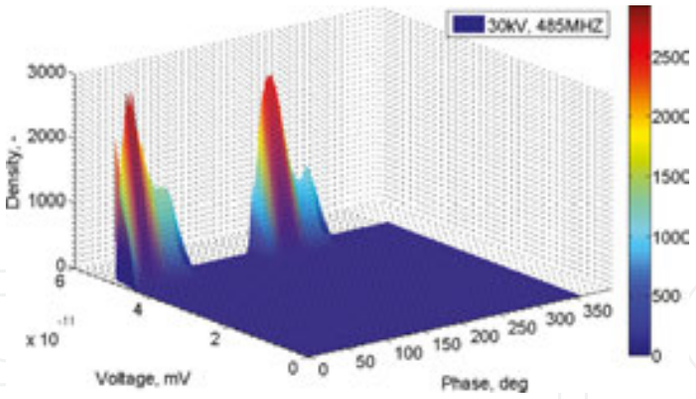

Figure 23. Voltages measured at f = 485 MHz.

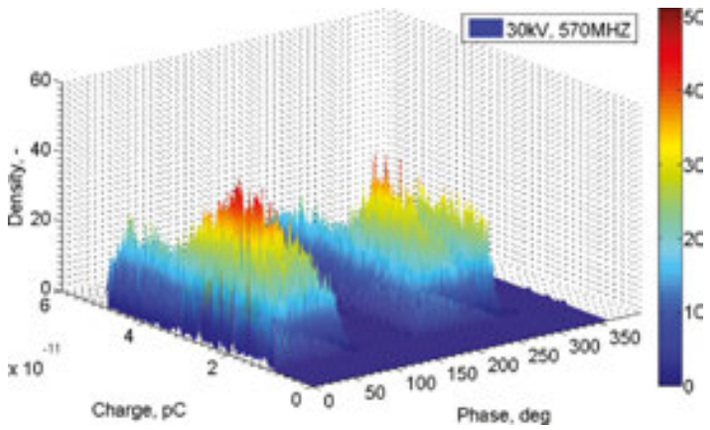

Figure 24. Charges measured at f = 570.MHz.

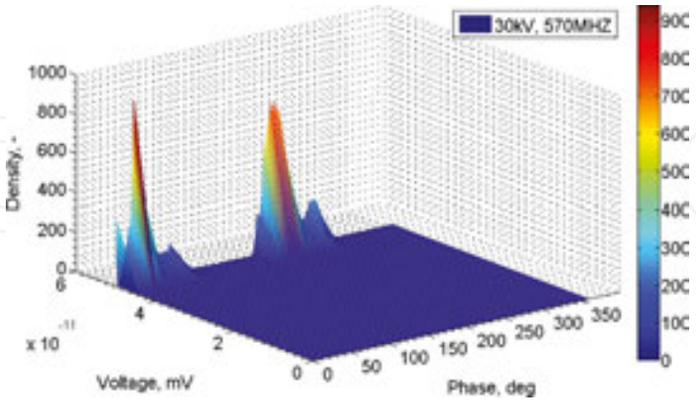

Figure 25. Voltages measured at f = 570 MHz.

In **Figures 26–31**, the results of histograms calculated for the supply voltage phases over charges registered at a chosen frequency f = 570 MHz, while generating PD at various voltage levels in the SURF system, are presented.

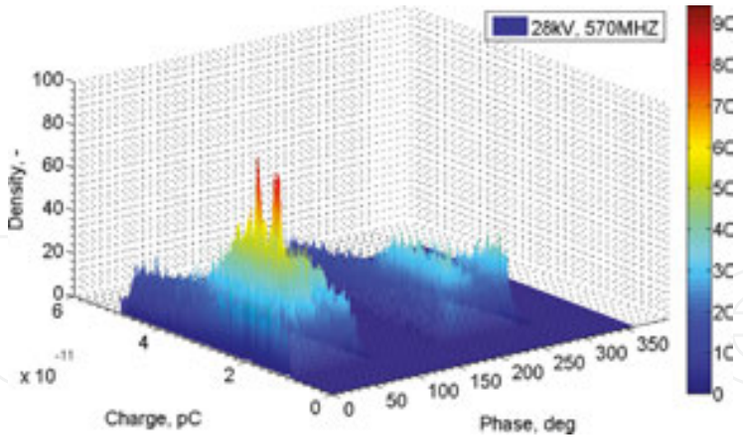

Figure 26. U = 28 kV.

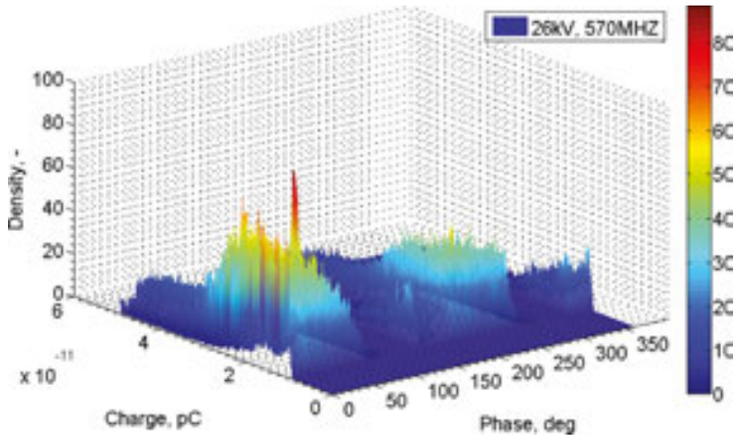

Figure 27. U = 26 kV.

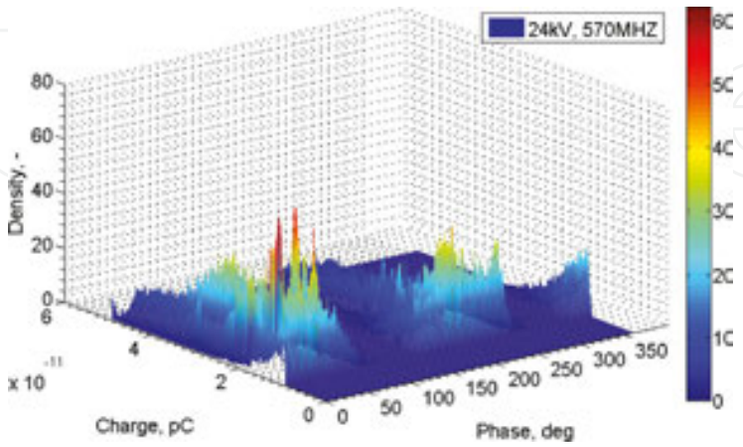

Figure 28. U = 24 kV.

http://dx.doi.org/10.5772/62409

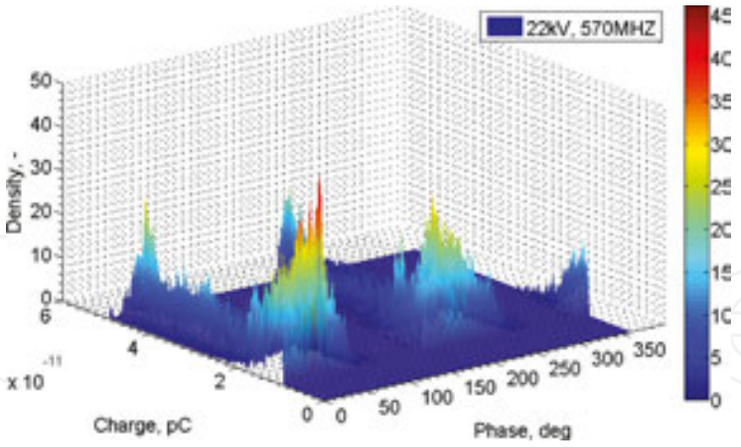

Figure 29. U = 22 kV.

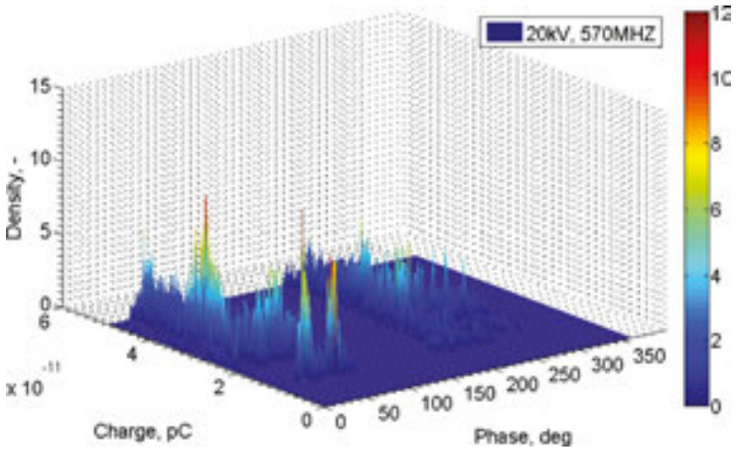

Figure 30. U = 20 kV.

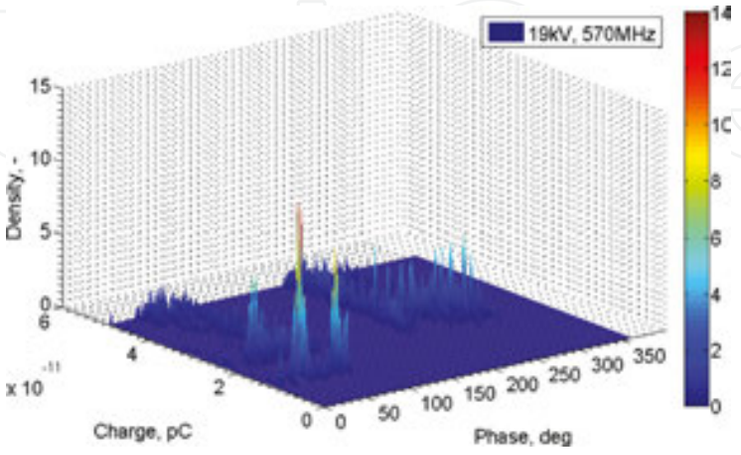

Figure 31. U = 19 kV.

In **Figures 32–34**, the results for histograms calculated for the supply voltage phases over charges registered while generating PD at U = 56 kV for various frequencies f in the NNB system are presented. In this electrode system, it was observed that all charts are normally distributed independently of the supply voltage phase.

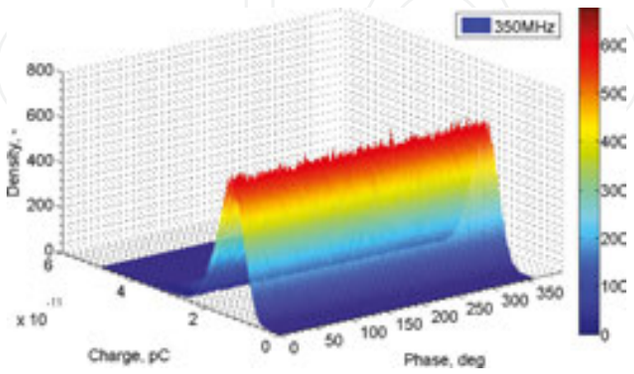

Figure 32. f = 350 MHz.

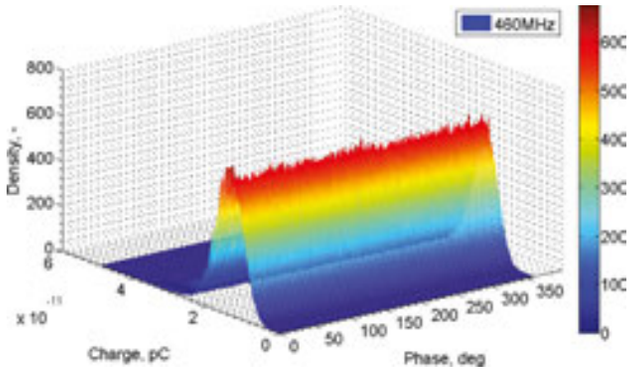

Figure 33. f = 460 MHz.

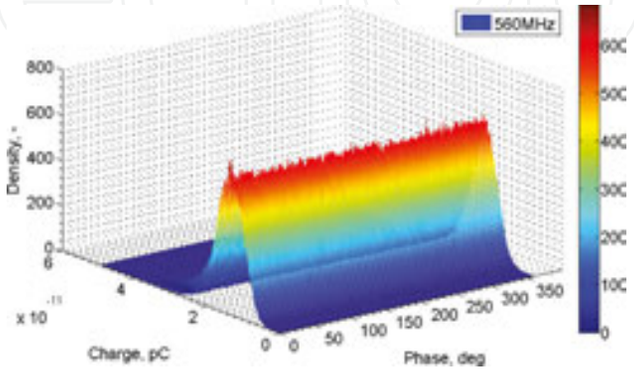

Figure 34. f = 560 MHz.

http://dx.doi.org/10.5772/62409

3.2. Results of analysis obtained using the spectrophotometry method

3.2.1. Results related to the needle-needle system

Measurements using the spectrophotometer were performed for different voltage values and at several distances between the measuring sensor and the PD generation area. In **Figures 35–37**, signals registered in the needle-needle system for distances 6, 7.5 and 8 mm are presented, respectively. Analysis of the charts resulted in the statement that there is no significant influence of the voltage value at the registered intensities at the three considered distances. The shape of the spectra remains similar when registered at the particular distances.

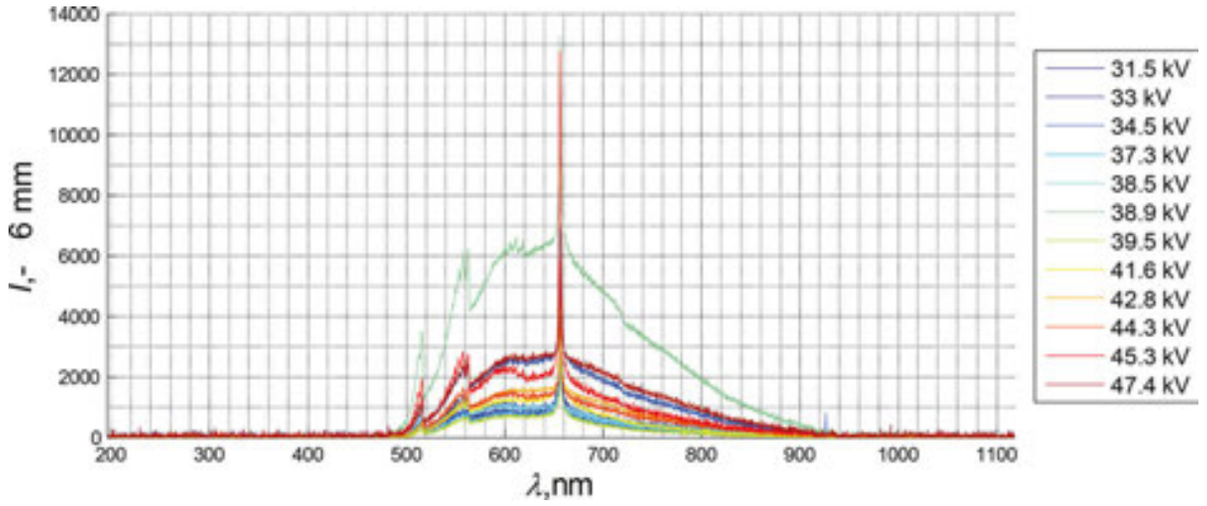

Figure 35. Spectra of the optical radiation emitted by PD generated at various supply voltage levels. The measuring sensor was placed at a distance equal to 6 mm from the HV electrode.

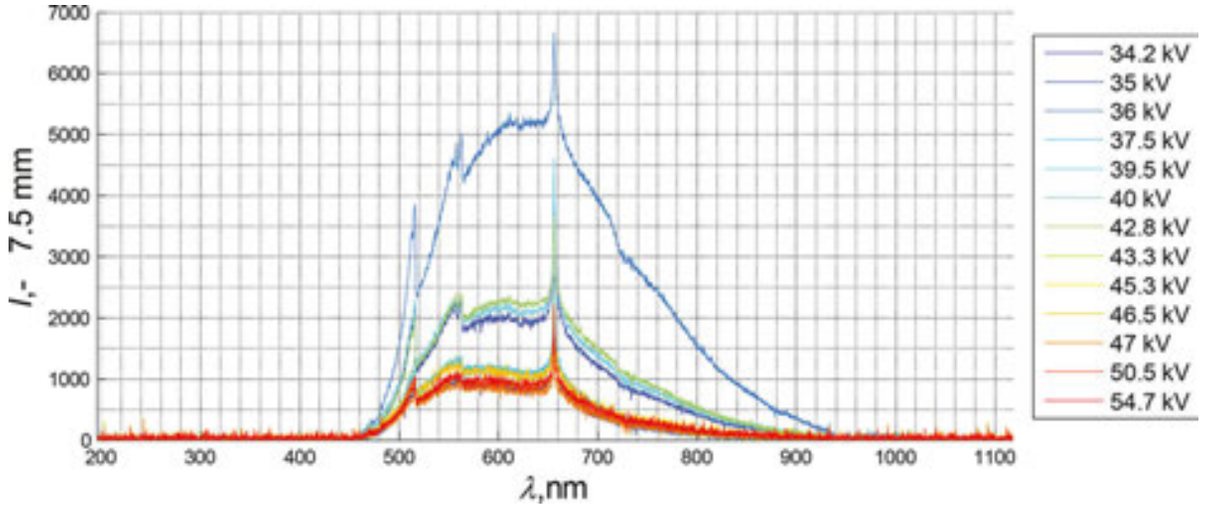

Figure 36. Spectra of the optical radiation emitted by PD generated at various supply voltage levels. The measuring sensor was placed at a distance equal to 7.5 mm from the HV electrode.

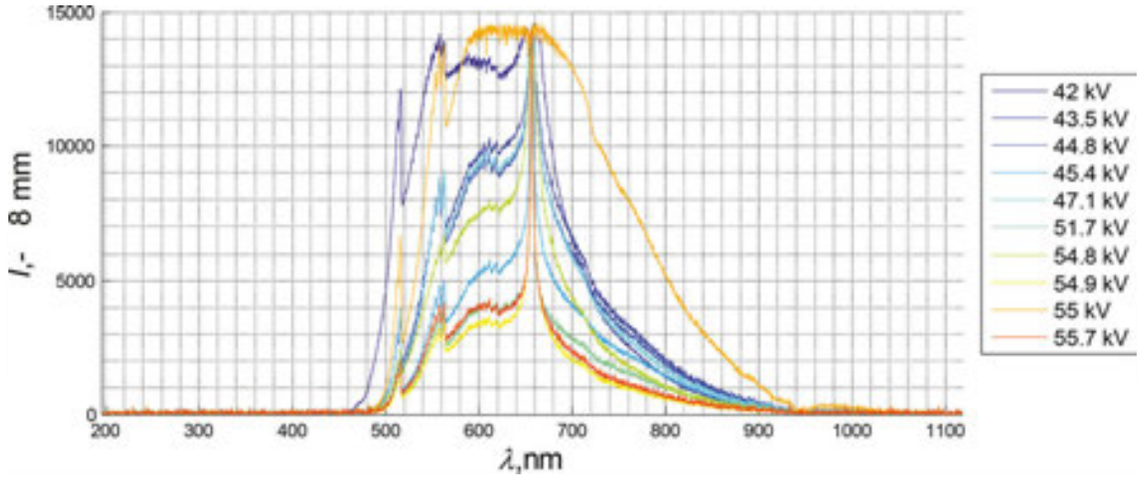

Figure 37. Spectra of the optical radiation emitted by PD generated at various supply voltage levels. The measuring sensor was placed at a distance equal to 8 mm from the HV electrode.

To confirm the above-mentioned visual analysis of voltage dependence, the maximal intensities in the registered spectra were selected for each of the trails. This type of analysis resulted in the presentation of the direct dependence of the intensity on the voltage, which is presented in **Figures 38–40** for the considered distances, respectively. In charts also, a linear approximation is presented together with the determination coefficient R^2, which was calculated from the Pearson equation.

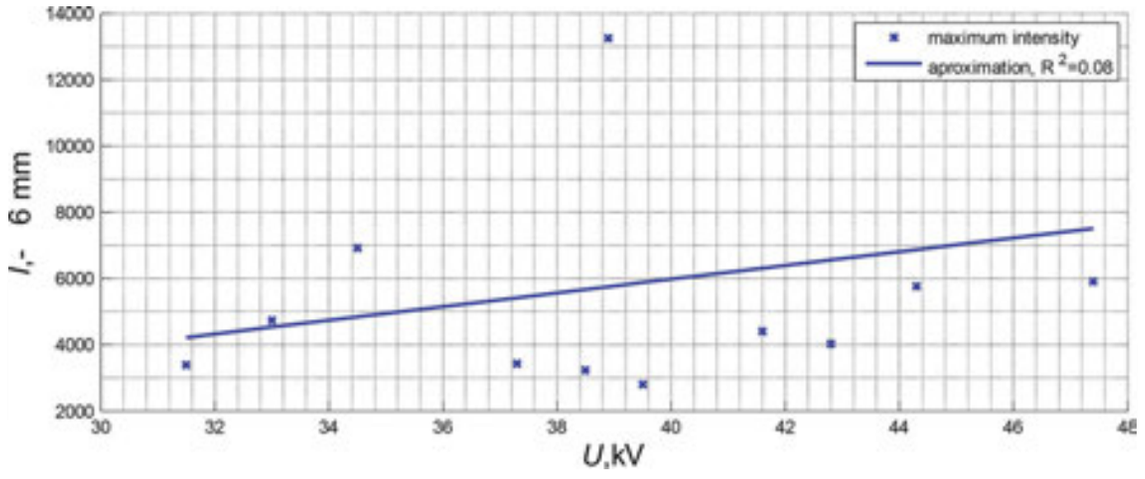

Figure 38. Maximal intensity registered at the distance 6 mm, in the function of PD generation voltage.

Analyzing the curve depicted in **Figure 38**, one may consider an increasing dependency of the voltage on intensity. Although the very low R^2 coefficient implies that the linear curve is not well-approximated. Reciprocal dependency was observed for data gathered at the distance of 7.5 (**Figure 39**) and 8 mm (**Figure 40**). In these cases, the R^2 values also imply low approximation quality. Based on the above, the lacking dependence of the voltage on the intensity was confirmed.

http://dx.doi.org/10.5772/62409

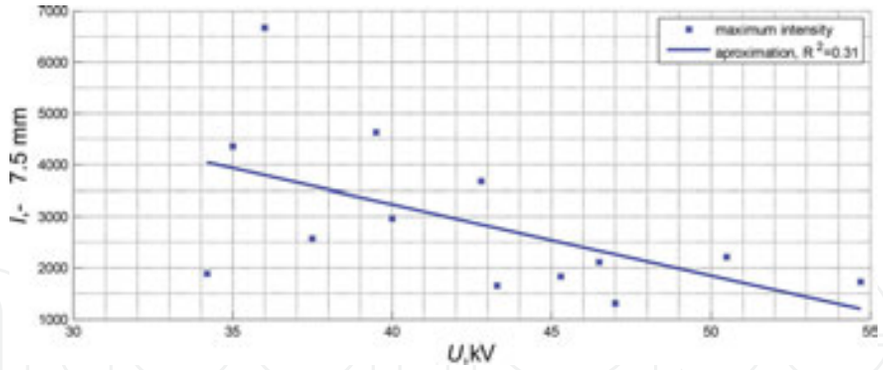

Figure 39. Maximal intensity registered at the distance 7.5 mm, in the function of PD generation voltage.

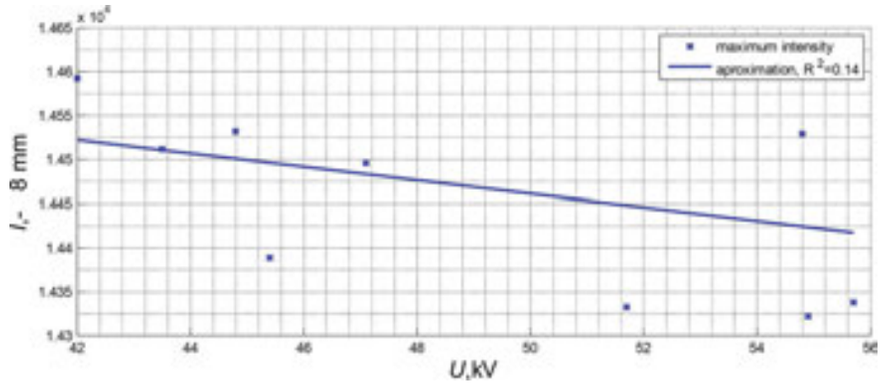

Figure 40. Maximal intensity registered at the distance 8 mm, in the function of PD generation voltage.

In the next step, the energy contained in the registered spectra was determined based on defined integrals calculated within the considered frequency range. In **Figures 41–43**, the estimated integrals in the function of supply voltage value are presented for the considered distances, respectively.

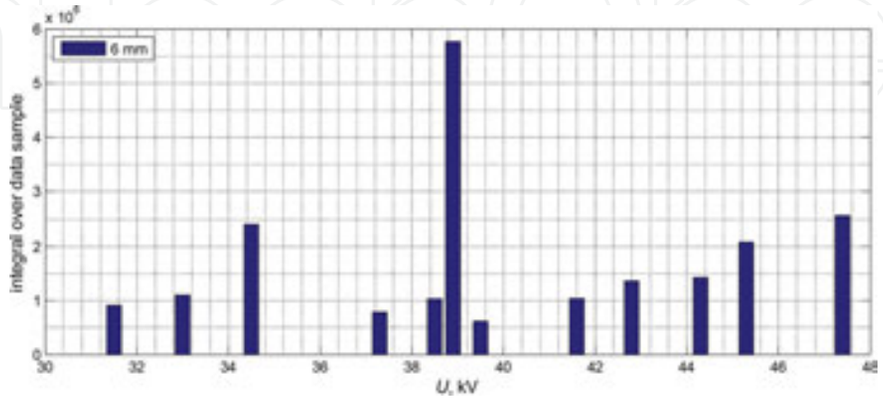

Figure 41. Integrals calculated for intensity spectra in the function of the PD generation voltage, while the sensor was installed at a distance equal to 6 mm.

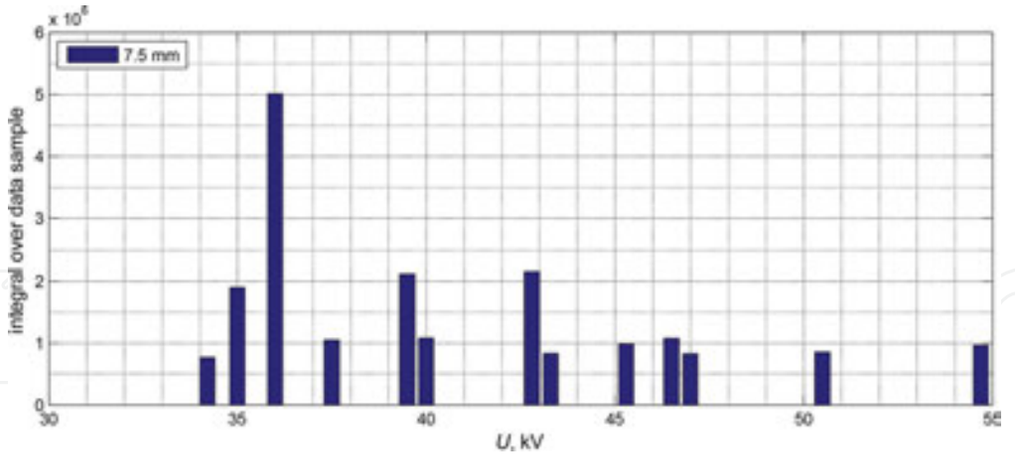

Figure 42. Integrals calculated for intensity spectra in the function of the PD generation voltage, while the sensor was installed at a distance equal to 7.5 mm.

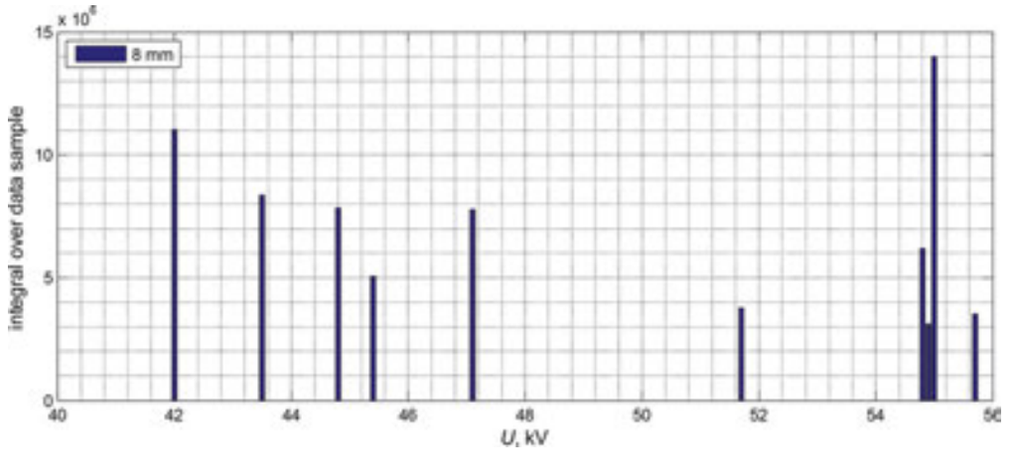

Figure 43. Integrals calculated for intensity spectra in the function of the PD generation voltage, while the sensor was installed at a distance equal to 8 mm.

At the distance of 6 mm, the highest energy was estimated for spectra registered at a supply voltage U = 39 kV. At the distance of 7.5 mm, the highest energy was estimated for spectra registered at a supply voltage U = 36 kV. At the distance of 8 mm, the highest energy was estimated for spectra registered at a supply voltage U = 55 kV. No significant dependency of the voltage value on the energy was recognized, contained in the spectra regardless of the distance at which the measuring sensor was installed.

3.2.2. Results related to the needle-needle system with air bubbles

In **Figures 44–47**, signals registered in the needle-needle system with air bubbles for distances 5, 6, 7.5 and 8 mm are presented, respectively. Analyses of the charts resulted with the same statement, as it was the case of NN system, namely, that there is no significant influence of the voltage value on the registered intensities at the considered distances. The shape of the spectra

http://dx.doi.org/10.5772/62409

remains similar when registered at the particular distances and is also very similar as it was the case of NN system.

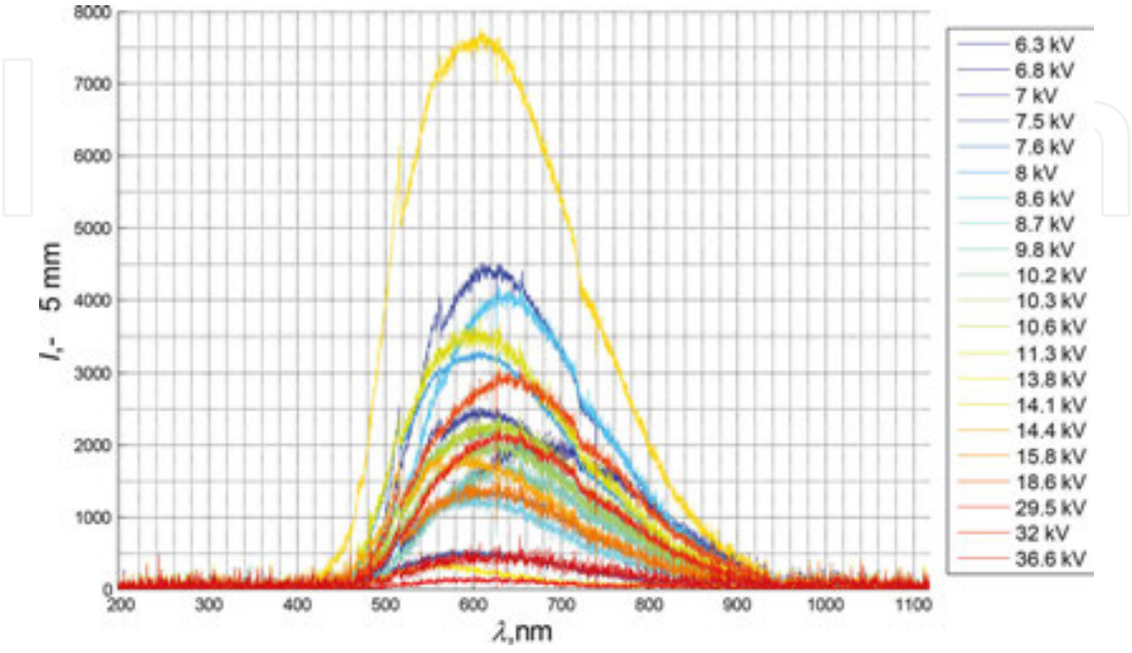

Figure 44. Spectra of the optical radiation emitted by PD generated at various supply voltage levels. The measuring sensor was placed at a distance equal to 5 mm from the HV electrode.

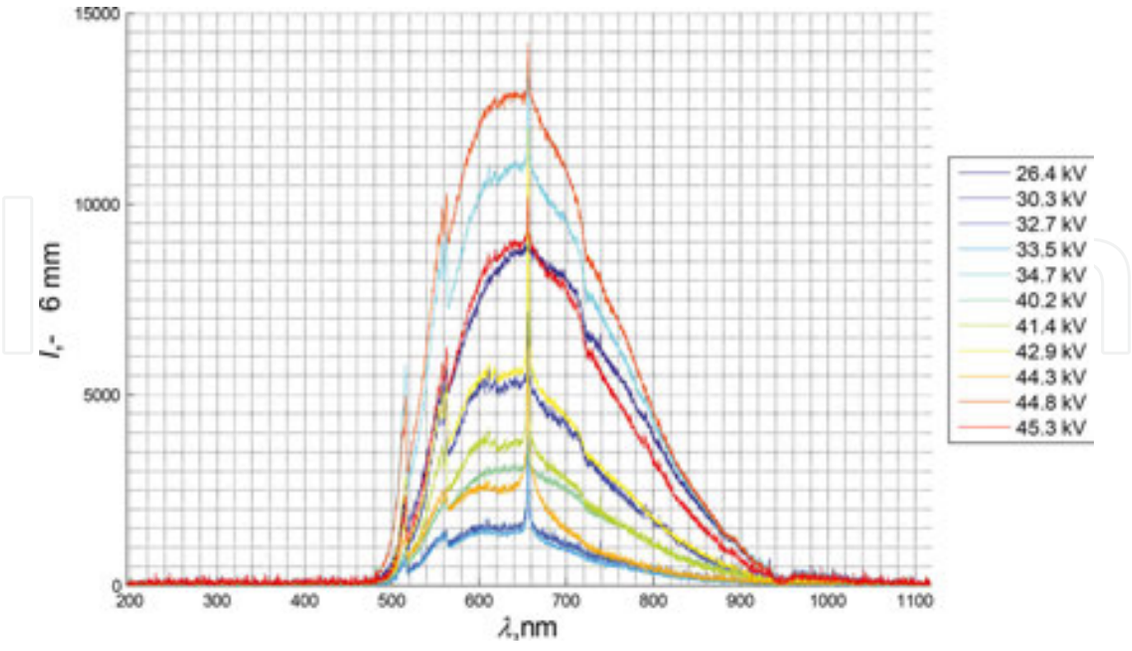

Figure 45. Spectra of the optical radiation emitted by PD generated at various supply voltage levels. The measuring sensor was placed at a distance equal to 6 mm from the HV electrode.

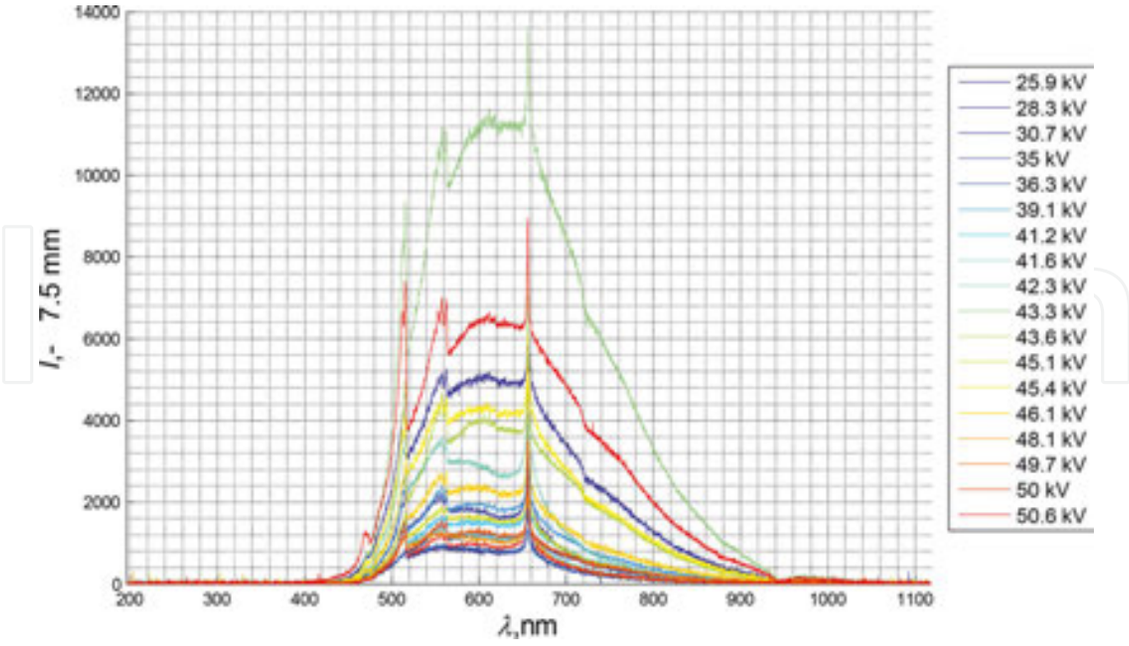

Figure 46. Spectra of the optical radiation emitted by PD generated at various supply voltage levels. The measuring sensor was placed at a distance equal to 7.5 mm from the HV electrode.

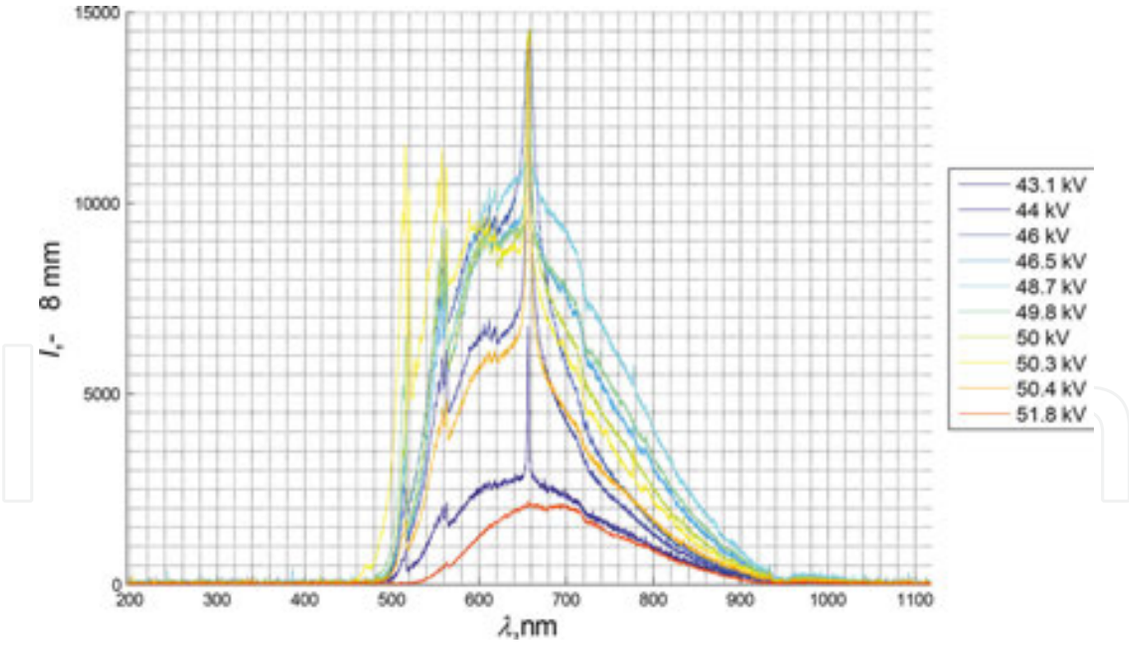

Figure 47. Spectra of the optical radiation emitted by PD generated at various supply voltage levels. The measuring sensor was placed at a distance equal to 8 mm from the HV electrode.

Based on the relationships, depicted in **Figures 48–51**, the lacking dependency of the voltage on the registered intensities for the considered distances was confirmed.

http://dx.doi.org/10.5772/62409

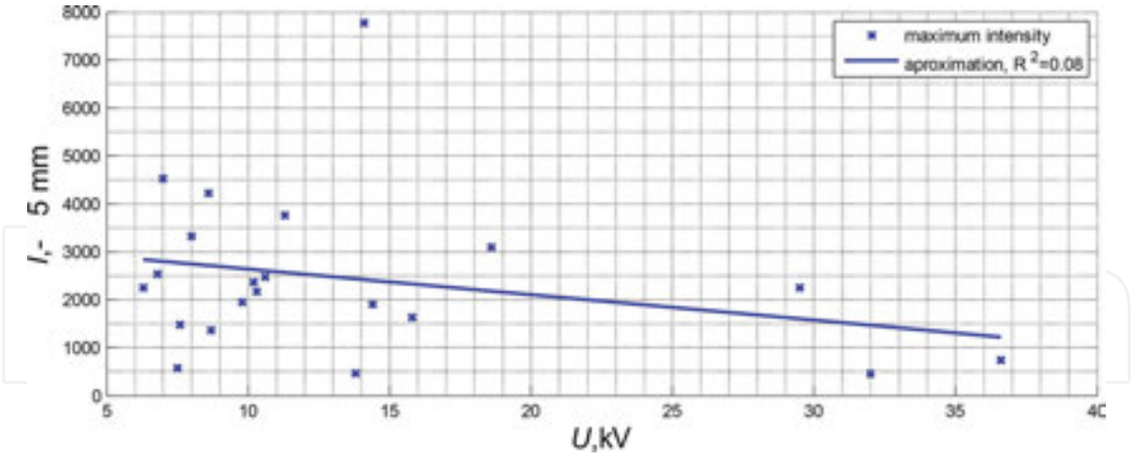

Figure 48. Maximal intensity registered at the distance 5 mm, in the function of PD generation voltage.

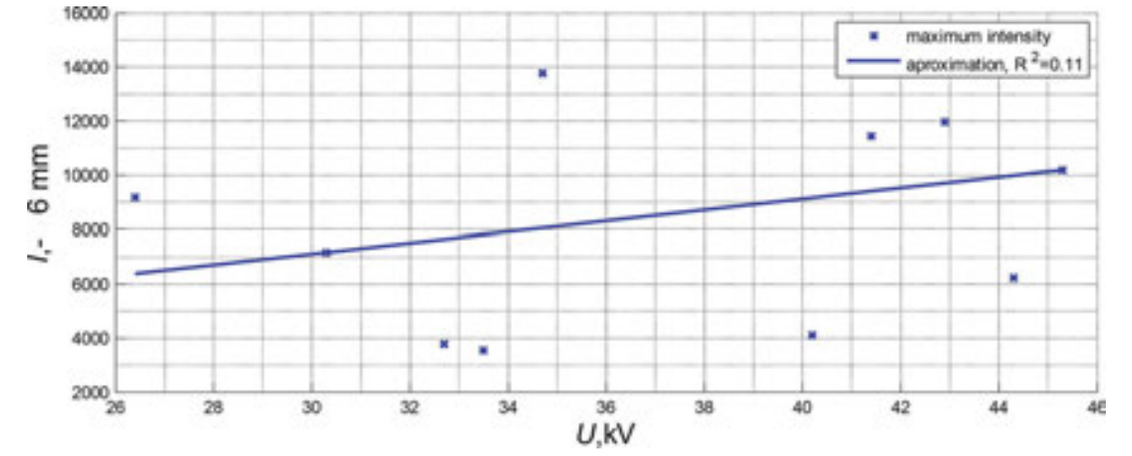

Figure 49. Maximal intensity registered at the distance 6 mm, in the function of PD generation voltage.

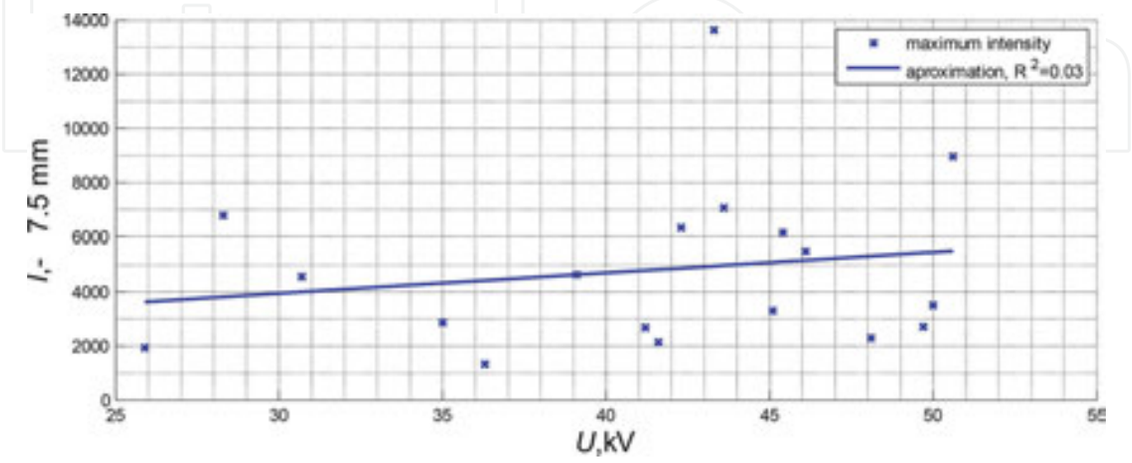

Figure 50. Maximal intensity registered at the distance 7.5 mm, in the function of PD generation voltage.

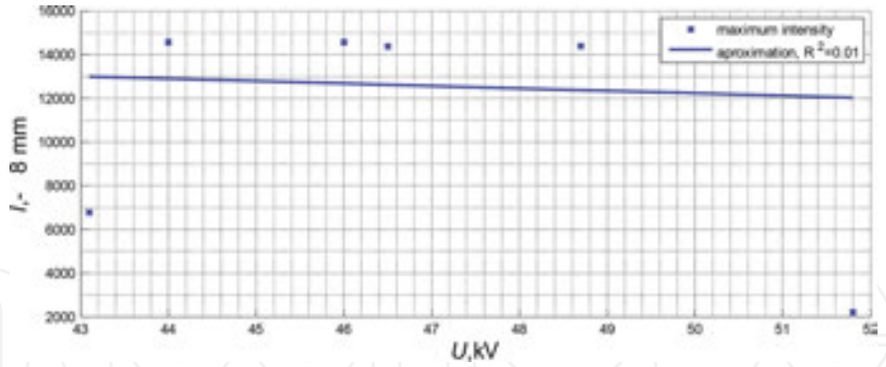

Figure 51. Maximal intensity registered at the distance 8 mm, in the function of PD generation voltage.

The energy values contained in the registered spectra were determined for the analyzed supply voltage levels. The calculation results are presented in **Figures 52–55** for the considered distances, respectively.

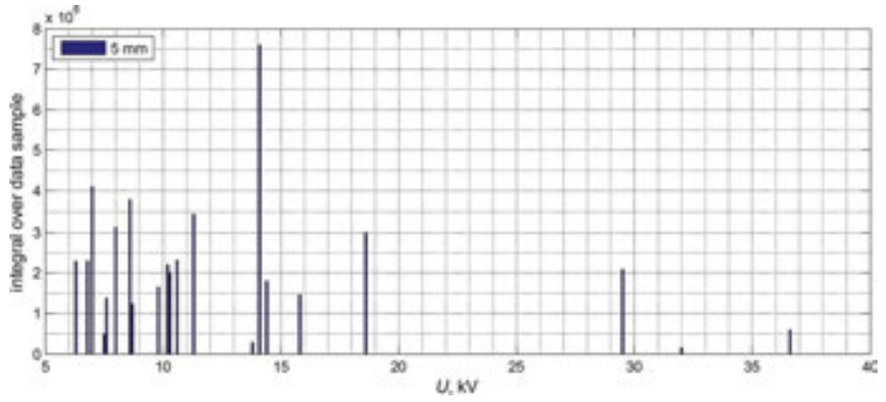

Figure 52. Integrals calculated for intensity spectra in the function of the PD generation voltage, while the sensor was installed at a distance equal to 5 mm.

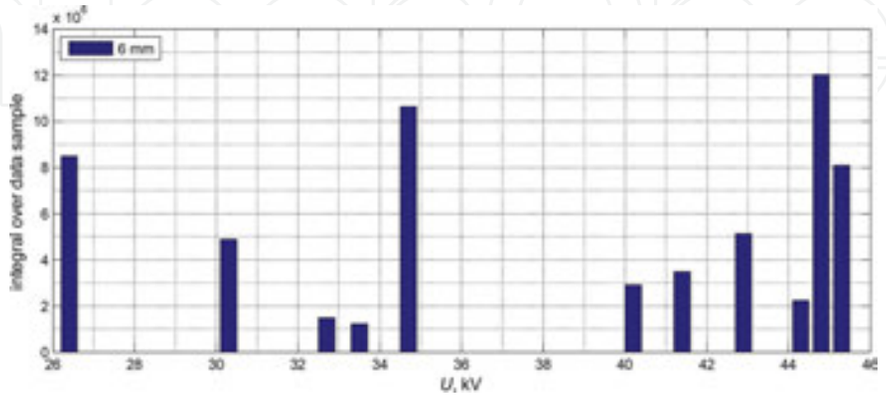

Figure 53. Integrals calculated for intensity spectra in the function of the PD generation voltage, while the sensor was installed at a distance equal to 6 mm.

http://dx.doi.org/10.5772/62409

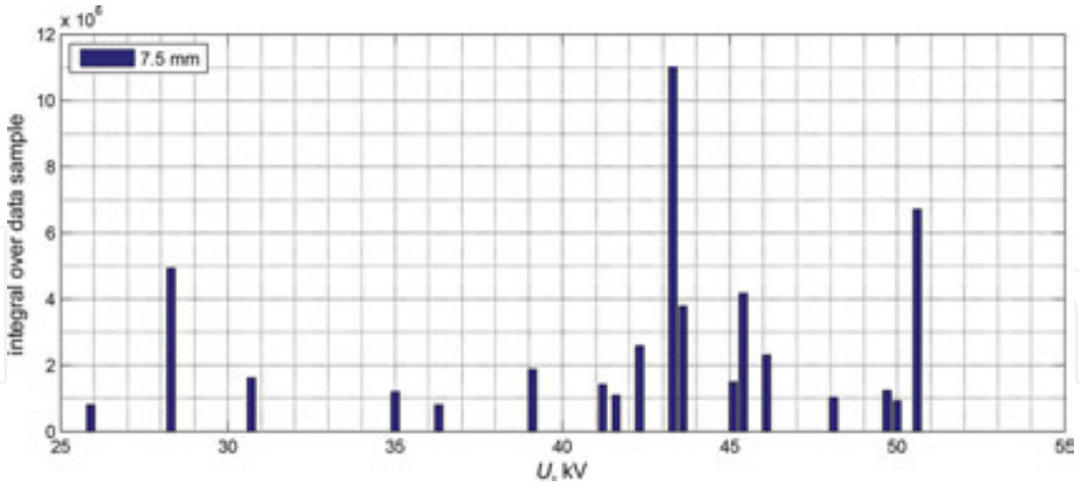

Figure 54. Integrals calculated for intensity spectra in the function of the PD generation voltage, while the sensor was installed at a distance equal to 7.5 mm.

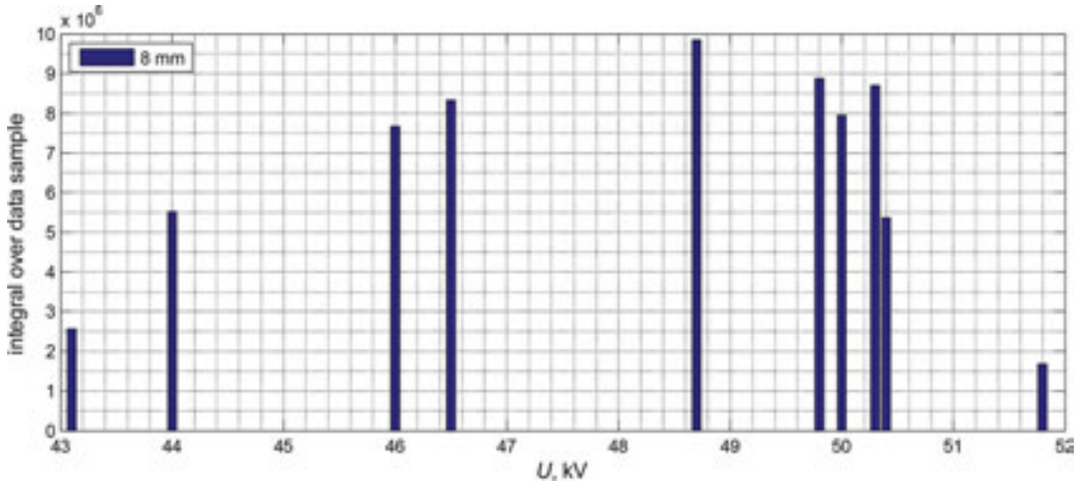

Figure 55. Integrals calculated for intensity spectra in the function of the PD generation voltage, while the sensor was installed at a distance equal to 8 mm.

At the distance of 8 mm, high energies were estimated for spectra registered at the supply voltage in the range from 46 to 51 kV. At the distance of 7.5 mm, the highest energy was estimated for spectra registered at a supply voltage U = 33 kV. At the distance of 6 mm, the highest energy was estimated for spectra registered at a supply voltage U = 45 kV. At the distance 5 mm, the highest energy was estimated for spectra registered at a supply voltage U = 14 kV. No significant dependency of the voltage value on the energy was recognized, contained in the spectra regardless of the distance at which the measuring sensor was installed.

3.2.3. Results related to the surface system

In contrast to the previously considered NN and NNB systems, in the SURF system a clear dependency of voltage on the registered intensity spectra was observed. In **Figures 56–58**,

intensities registered in the surface system for distances 4, 6 and 8 mm are presented, respectively. The shape of the spectra remains similar when registered at the particular distances.

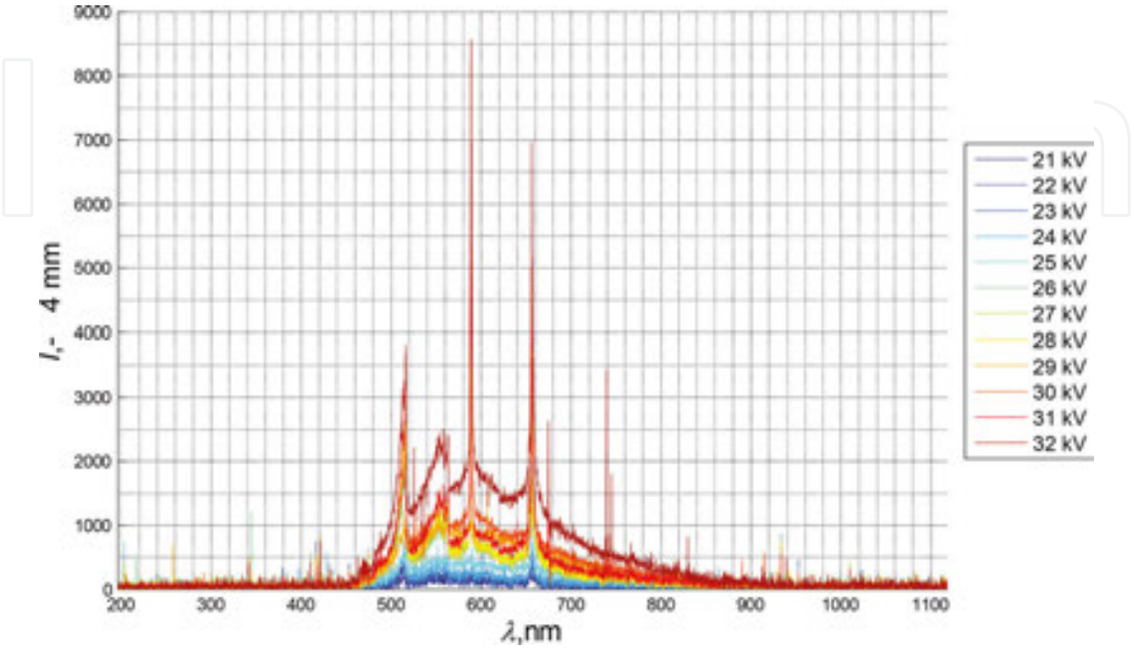

Figure 56. Spectra of the optical radiation emitted by PD generated at various supply voltage levels. The measuring sensor was placed at a distance equal to 4 mm from the HV electrode.

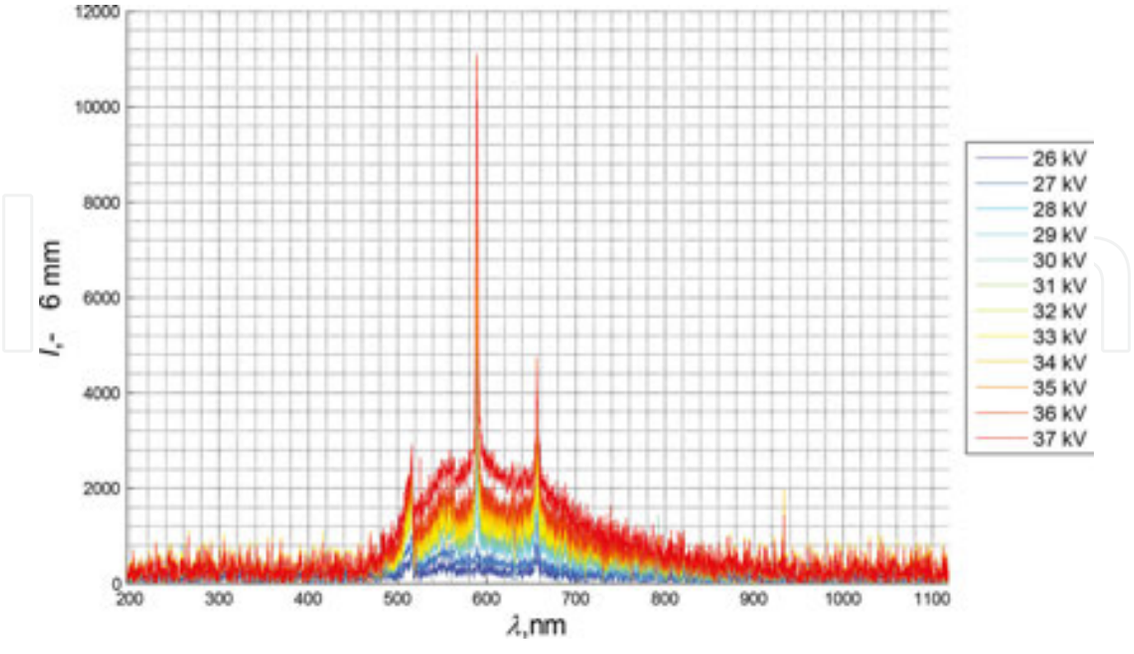

Figure 57. Spectra of the optical radiation emitted by PD generated at various supply voltage levels. The measuring sensor was placed at a distance equal to 6 mm from the HV electrode.

http://dx.doi.org/10.5772/62409

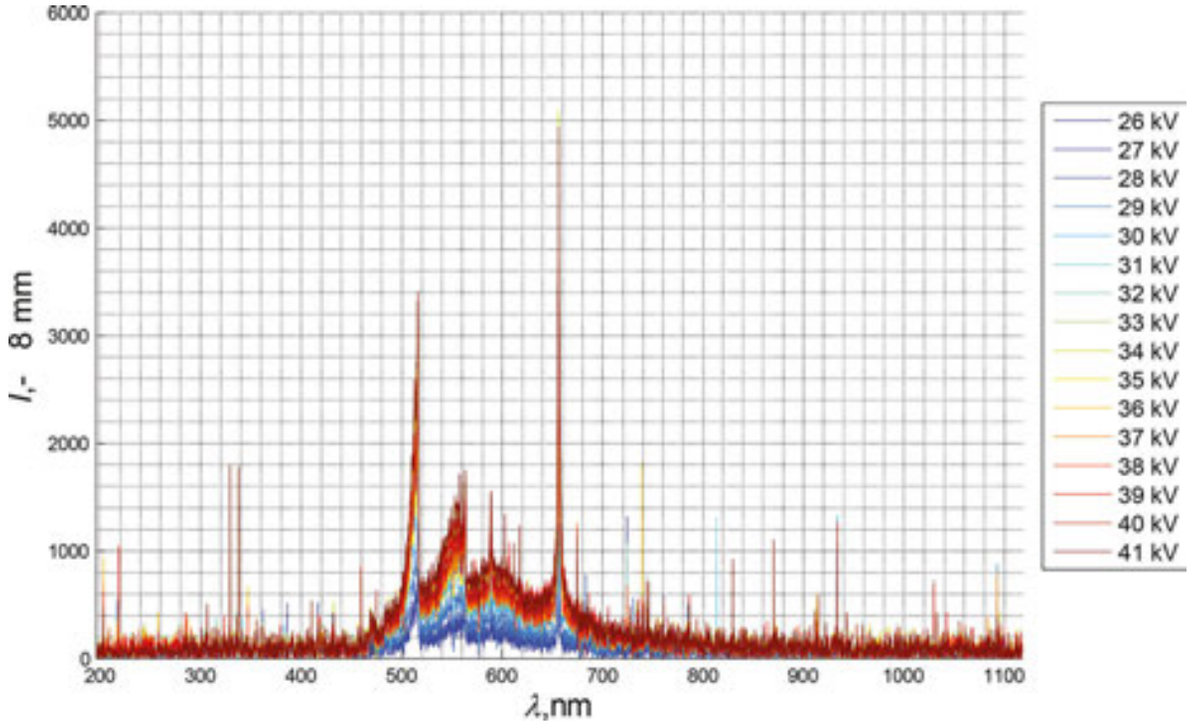

Figure 58. Spectra of the optical radiation emitted by PD generated at various supply voltage levels. The measuring sensor was placed at a distance equal to 8 mm from the HV electrode.

The above-mentioned clear observed dependency was confirmed by the relationships depicted in **Figures 59–61**. Also the linear approximation, which indicates higher R^2 values, confirms the given statement.

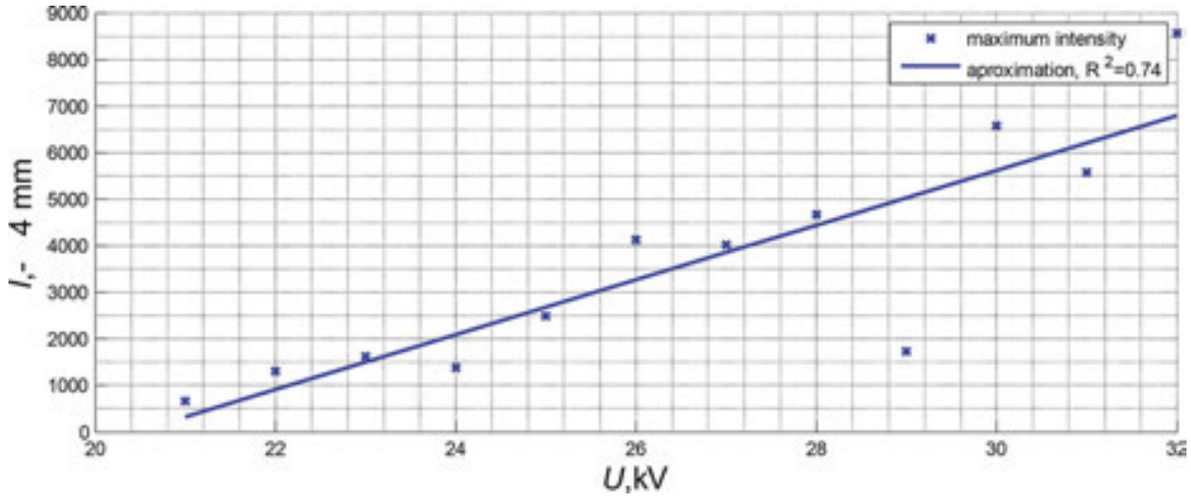

Figure 59. Maximal intensity registered at the distance 4 mm, in the function of PD generation voltage.

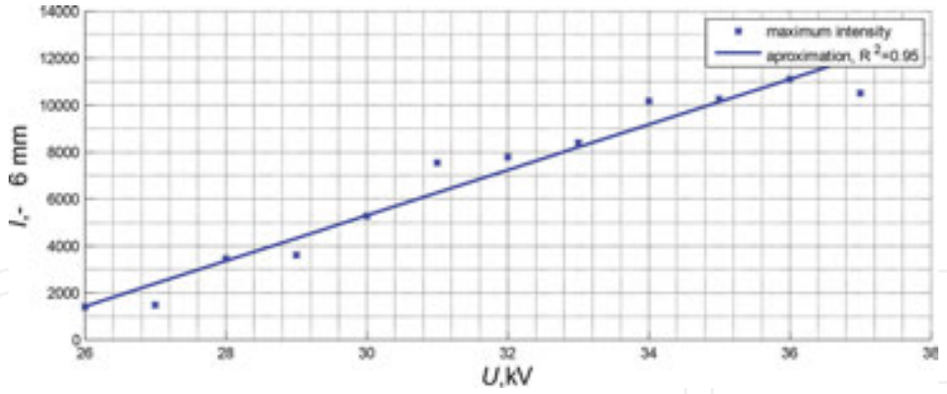

Figure 60. Maximal intensity registered at the distance 6 mm, in the function of PD generation voltage.

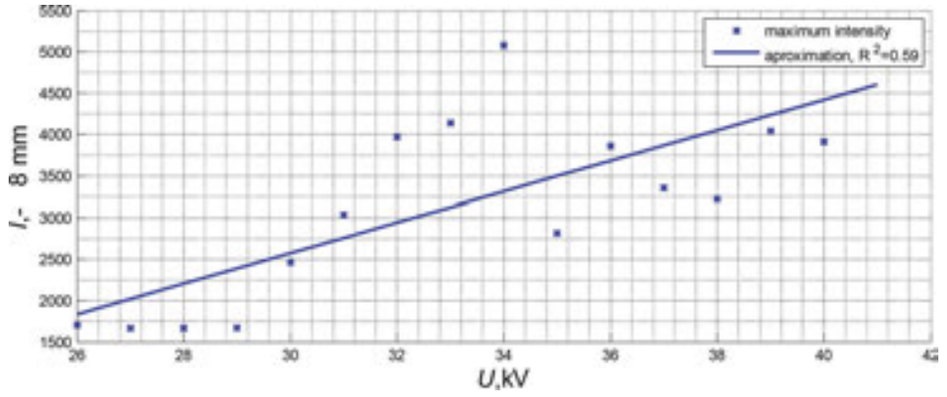

Figure 61. Maximal intensity registered at the distance 8 mm, in the function of PD generation voltage.

The energy values contained in the registered spectra were determined for the analyzed supply voltage levels. The calculation results are presented in **Figures 62–64** for the considered distances, respectively.

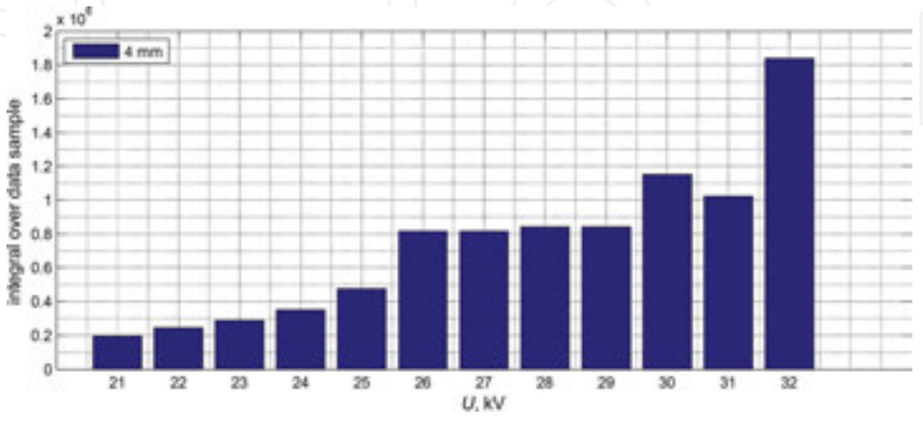

Figure 62. Integrals calculated for intensity spectra in the function of the PD generation voltage, while the sensor was installed at a distance equal to 4 mm.

http://dx.doi.org/10.5772/62409

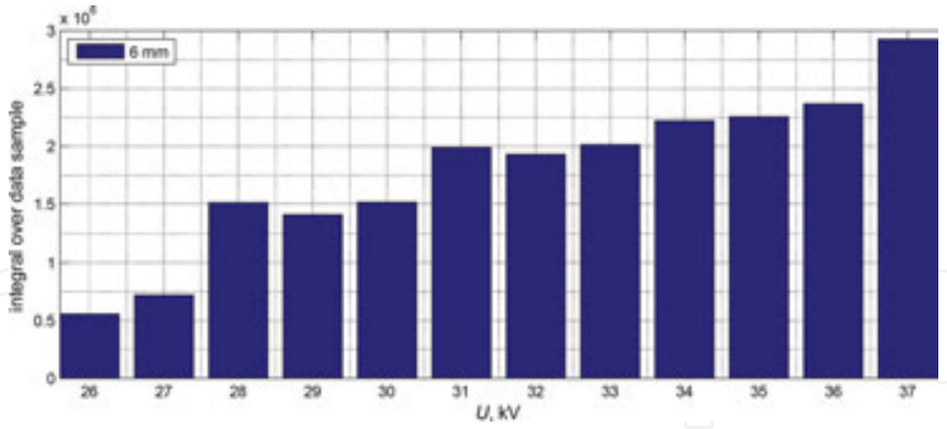

Figure 63. Integrals calculated for intensity spectra in the function of the PD generation voltage, while the sensor was installed at a distance equal to 6 mm.

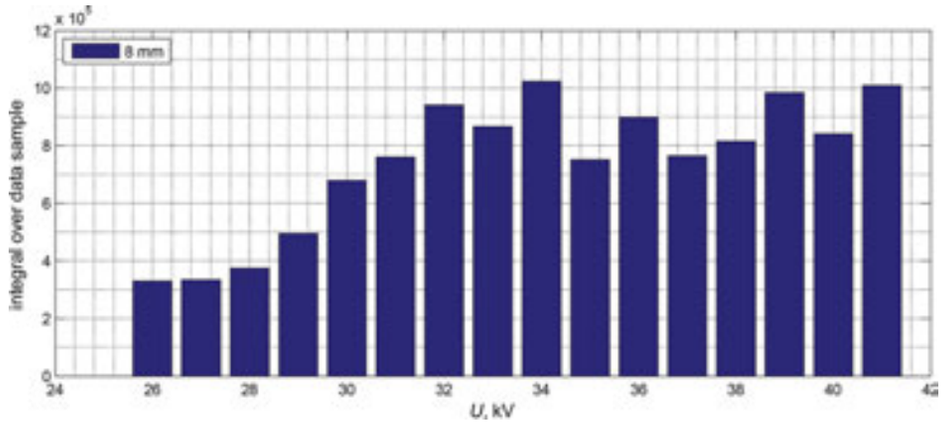

Figure 64. Integrals calculated for intensity spectra in the function of the PD generation voltage, while the sensor was installed at a distance equal to 8 mm.

Analysis of the energies calculated for the spectra registered at various distances enabled for the statement that these energies increase with the increasing value of PD generation voltage. Further, it was observed that at smaller distances (4 and 6 mm) the relationship is monotonic, despite to signals registered at 8 mm, where the energy remains almost constant, after the supply voltage achieves the value of 32 kV.

3.3 Results of analysis obtained using the acoustic emission method

For each of the regarded PD modelling systems and for various supply voltage values, over one hundred trails were recorded using the AE method. In the NN and SURF systems, a broad range of voltage values was analyzed, but for the NNB system only the 25 kV was involved. The results consider time runs and power spectral densities. In **Figures 65**, **67**, and **69**, time runs of AE signals registered while generating PD at selected voltage levels in the SURF, NN and NNB systems are presented, respectively. In **Figures 66**, **68**, and **70**, the corresponding

power spectral densities (PSD) are presented. For the PSD spectra, the local maxima (extreme values) were calculated and were marked with red crosses on the charts. These values were subjected for further analysis in the frequency domain.

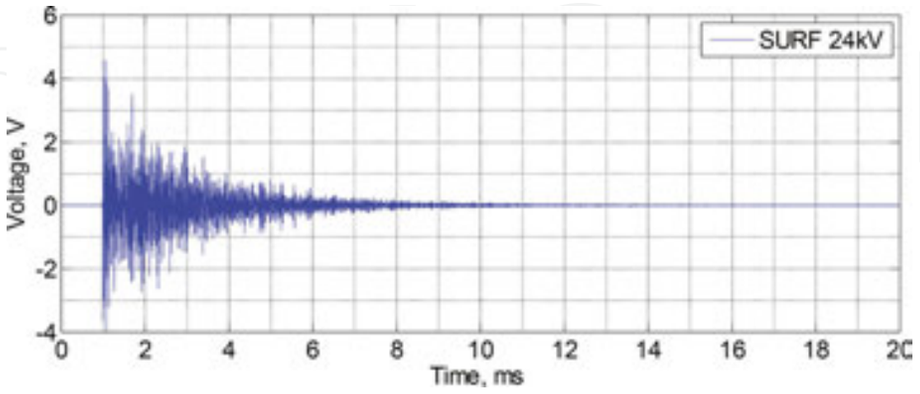

Figure 65. Time run of AE in the SURF system.

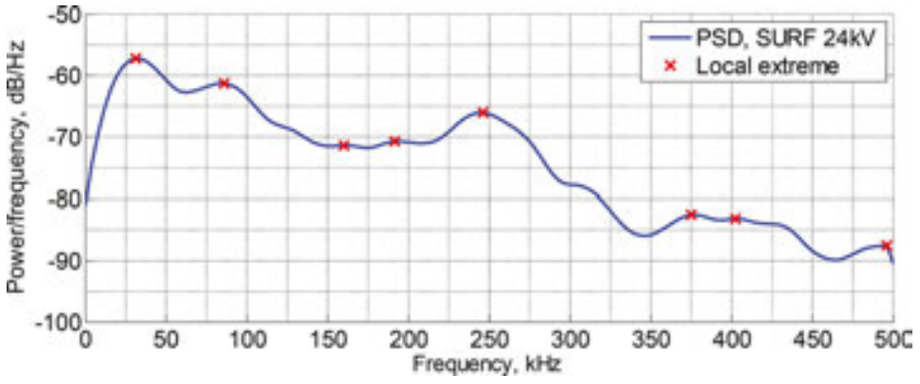

Figure 66. The corresponding PSD spectra.

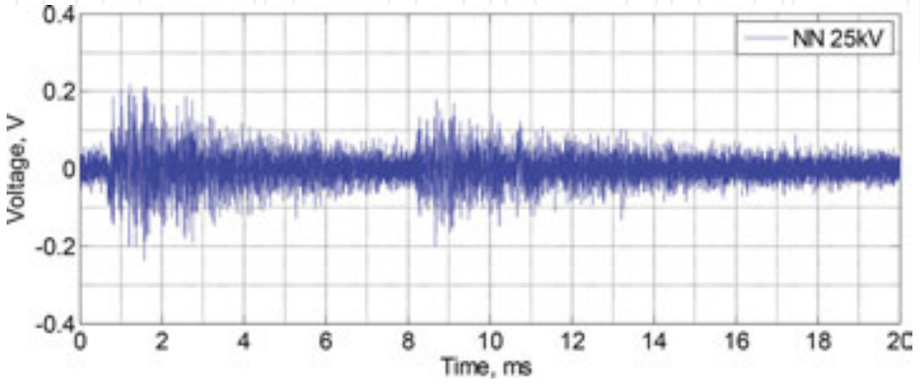

Figure 67. Time run of AE in the NN system.

http://dx.doi.org/10.5772/62409

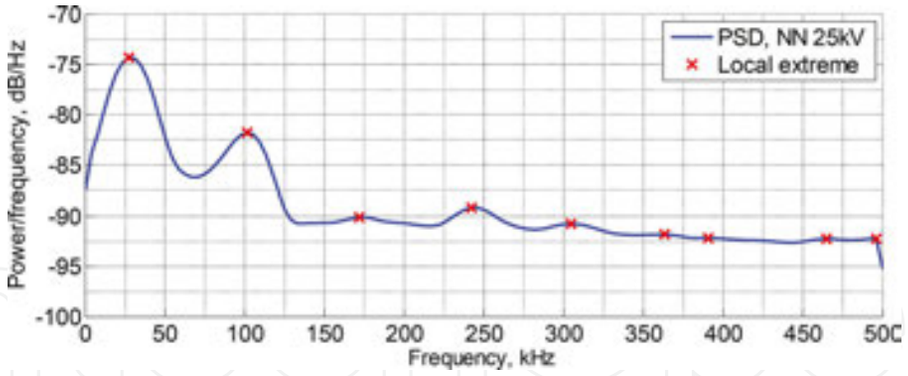

Figure 68. The corresponding PSD spectra.

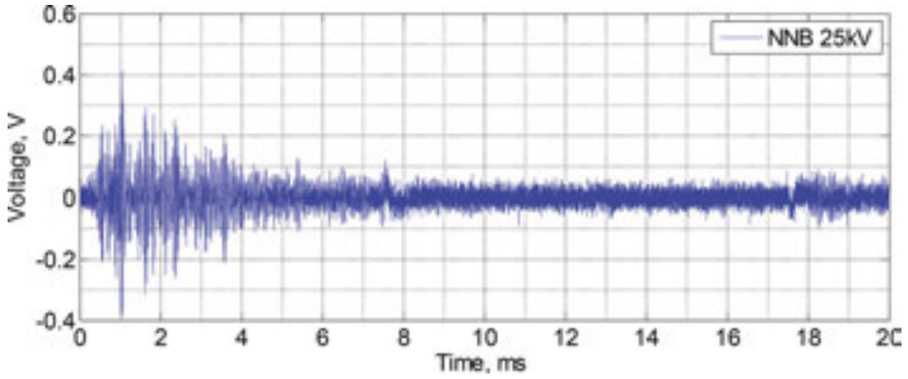

Figure 69. Time run of AE in the NNB system.

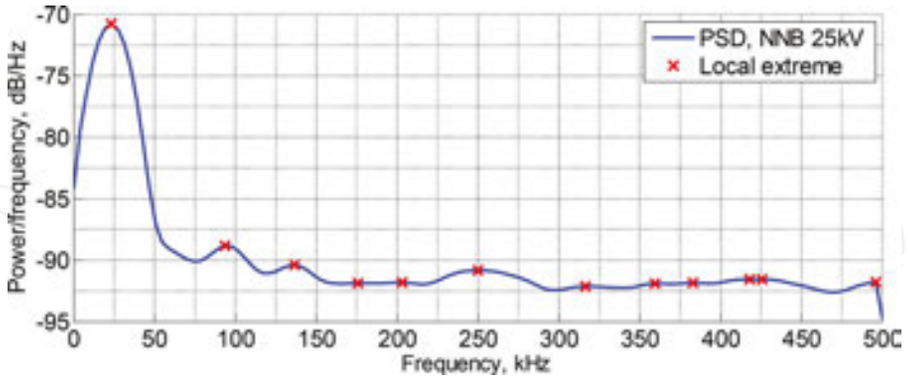

Figure 70. The corresponding PSD spectra.

The above-mentioned local extremes were subjected for empirical distribution analysis (histograms) with respect to the particular frequency values contained in the PSD spectra. In **Figures 71–73**, example results are presented for the three electrodes arrangements: NN (**Figure 71**), SURF (**Figure 72**), and NNB(**Figure 73**). The charts depict the distributions of local extremes in the PSD spectra, calculated for all measured data samples.

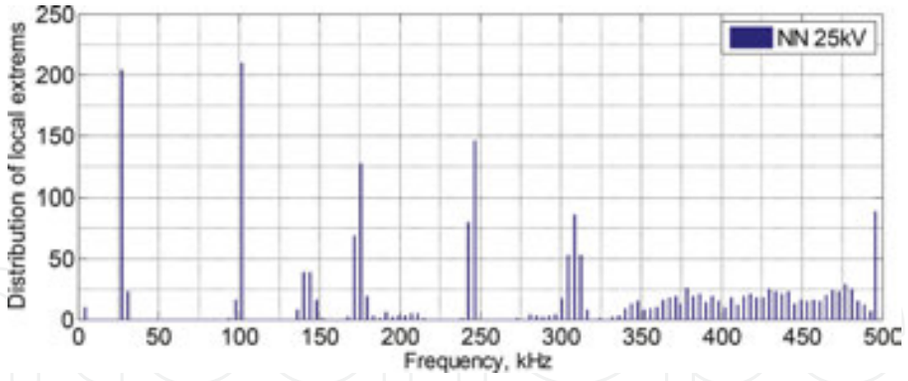

Figure 71. Empirical distributions (histograms) of local extreme values determined for all PSD spectra with respect to frequency for the NN system.

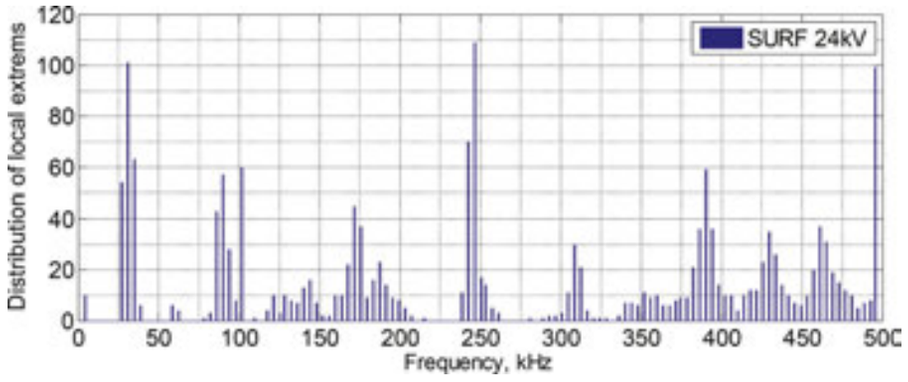

Figure 72. Empirical distributions (histograms) of local extreme values determined for all PSD spectra with respect to frequency for the SURF system.

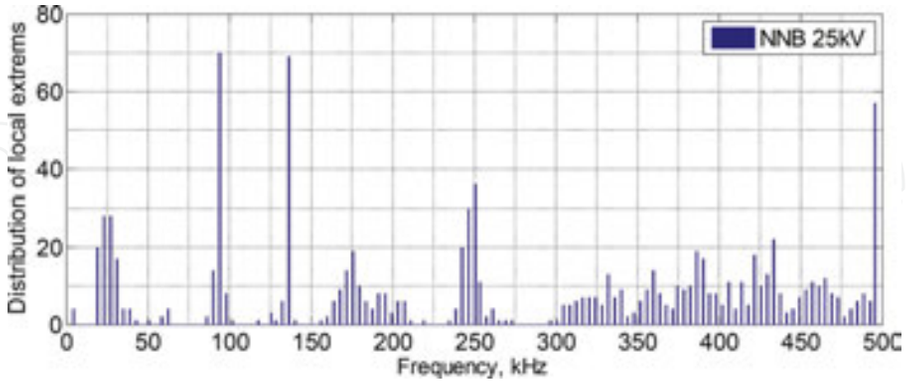

Figure 73. Empirical distributions (histograms) of local extreme values determined for all PSD spectra with respect to frequency for the NNB system.

For better comparison purposes, the particular charts were combined into a single figure, what has made possible to observe if any dependency of the PD generation voltage on the achieved results exists. In **Figures 74–75**, the mentioned relationships for the NN (**Figure 74**) and SURF

http://dx.doi.org/10.5772/62409

(**Figure 45**) are depicted. From the charts presented, it may be implied that there is no significant influence of PD generation voltage on the frequency components included in the PSD spectra, which were previously calculated for the AE signals registered in the NN and SURF system.

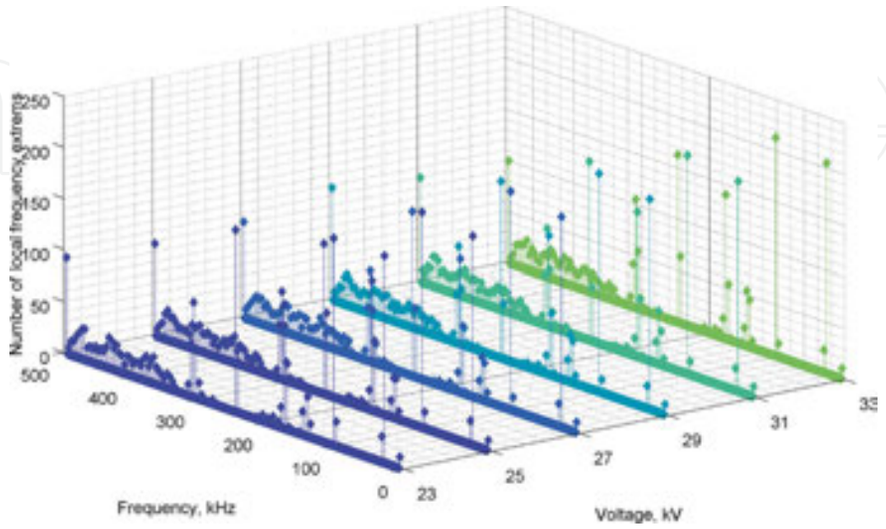

Figure 74. Relationship between PD generation voltage and the empirical distribution of local extreme values determined from the PSD spectra of AE signals registered in the NN system.

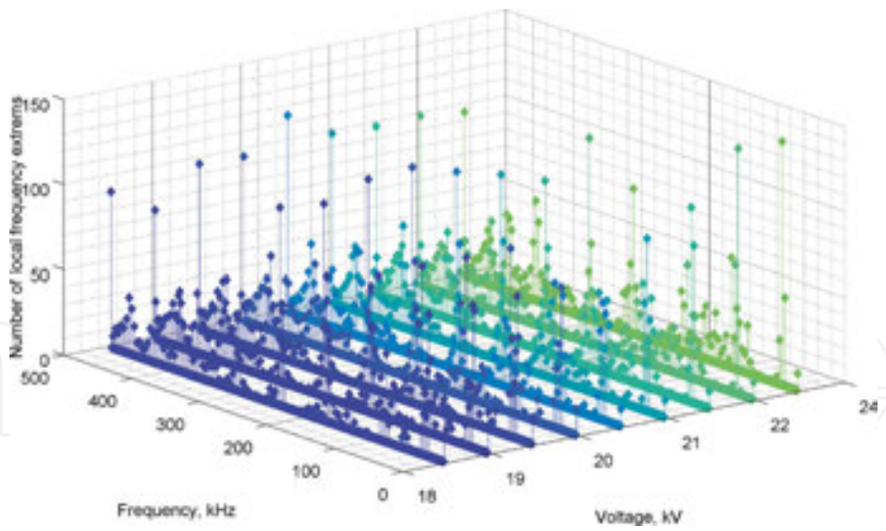

Figure 75. Relationship between PD generation voltage and the empirical distribution of local extreme values determined from the PSD spectra of AE signals registered in the SURF system.

3.4 Results of analysis obtained using the thermal imaging

The thermal imaging method was applied for all the earlier described measuring setups. Based on the results achieved, it was stated that there is no significant increase of temperature after

such a long time as 8 hours. Since the applied camera was not able to be immersed in the insulation oil, the eventual temperature variations, which are supposed to occur in the vicinity of the PD generation area, were not possible to detect during the performed research. In **Figures 76–77**, the example result of thermal image and the corresponding photo made in the visible frequency range are presented.

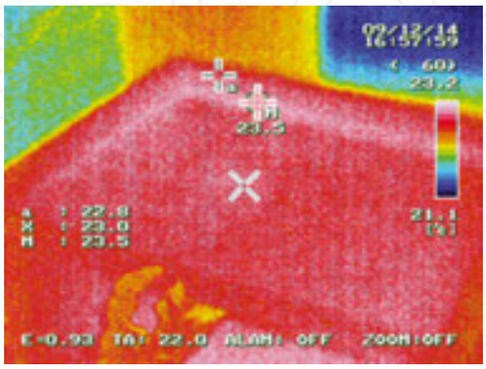

Figure 76. Example image made with the thermal camera.

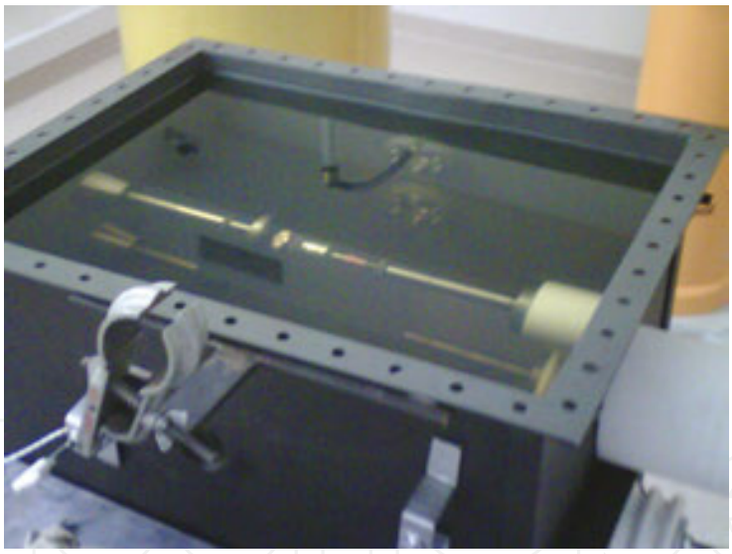

Figure 77. The corresponding photo of the investigated object.

3.5 Results of analysis obtained using the chromatography method

In order to analyze the chemical parameters of the insulating oil applied in the research, six oil samples were collected: first sample — at the beginning of the study, second sample — after 3 hours of PD generation, third, fourth, fifth and sixth samples — each after subsequent hour of PD generation. In **Figures 78–91**, the dendencies are presented showing the influence of PD generation time on selected parameters determined using the chromatography method.

http://dx.doi.org/10.5772/62409

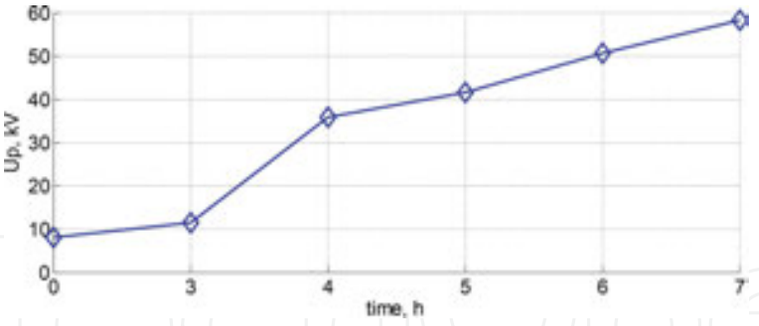

Figure 78. Up.

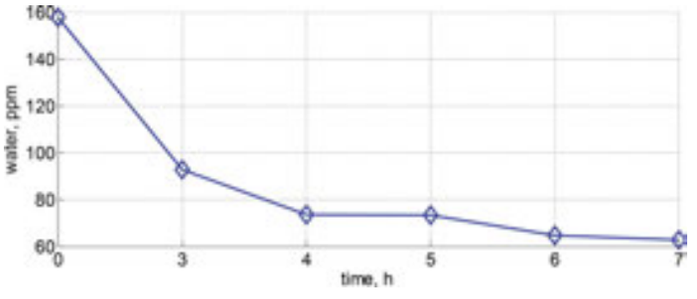

Figure 79. Water.

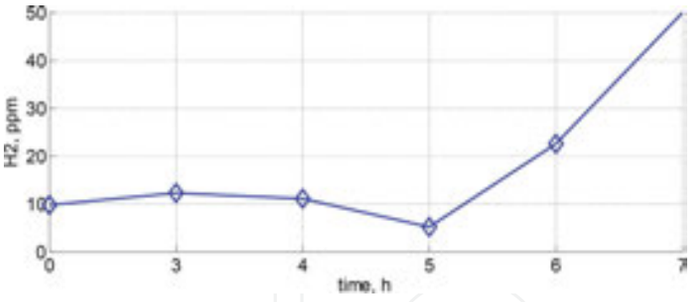

Figure 80. H2.

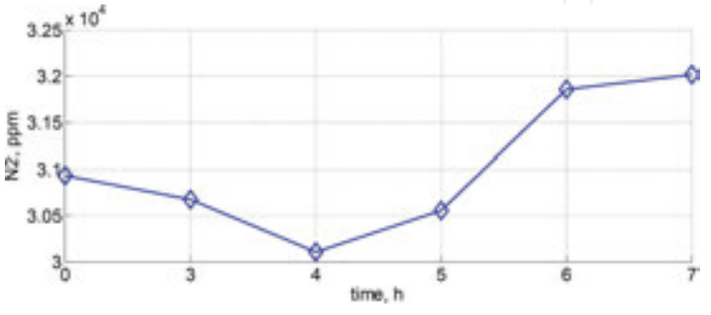

Figure 81. N2.

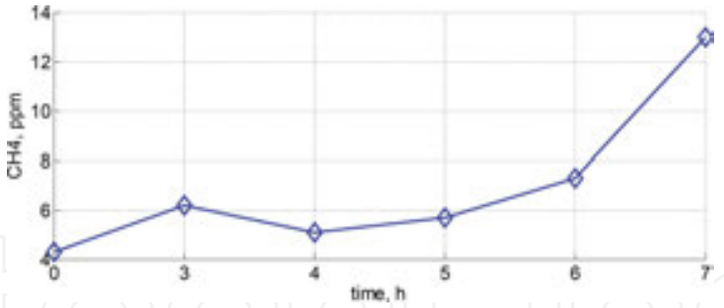

Figure 82. CH4.

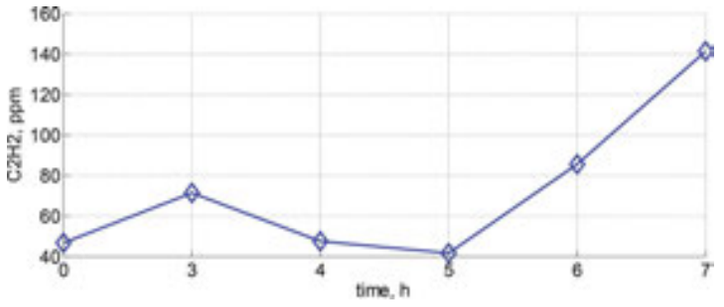

Figure 83. C2H2.

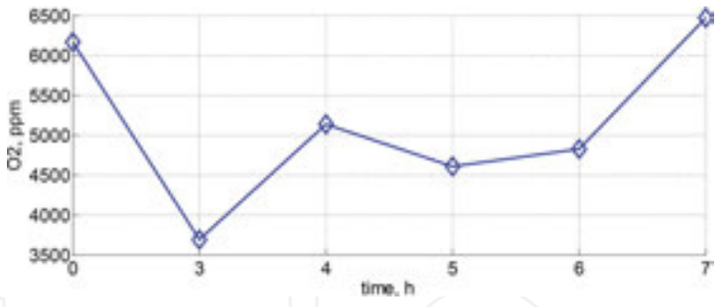

Figure 84. O2.

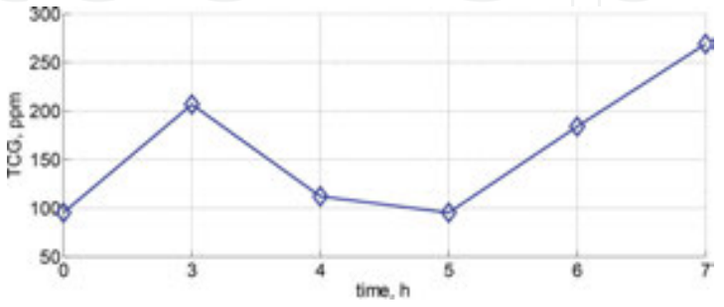

Figure 85. TCG.

http://dx.doi.org/10.5772/62409

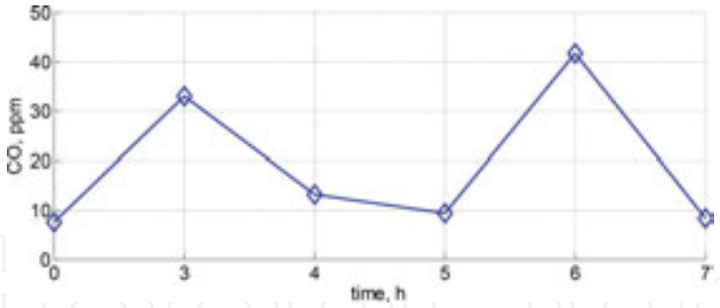

Figure 86. CO.

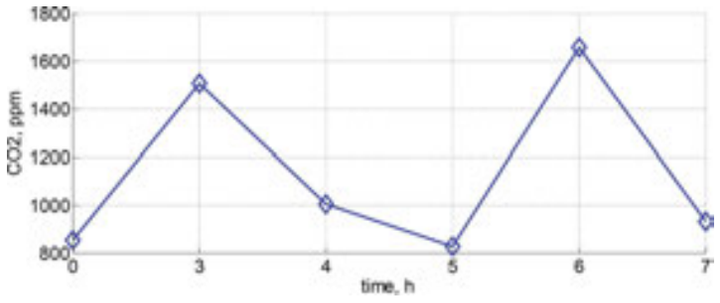

Figure 87. CO2.

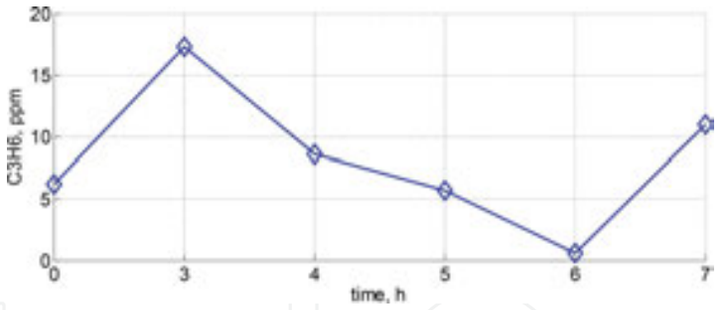

Figure 88. C3H6.

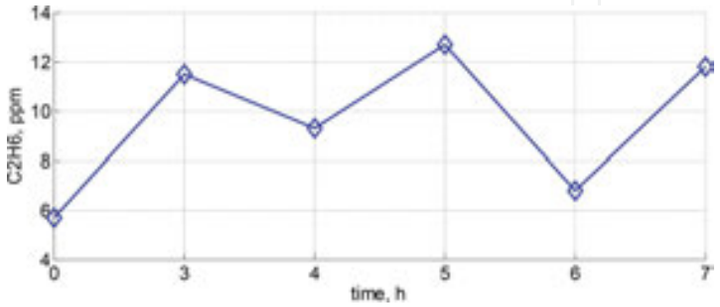

Figure 89. C2H6.

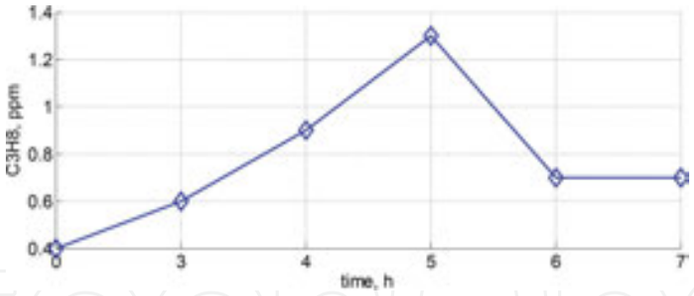

Figure 90. C3H8.

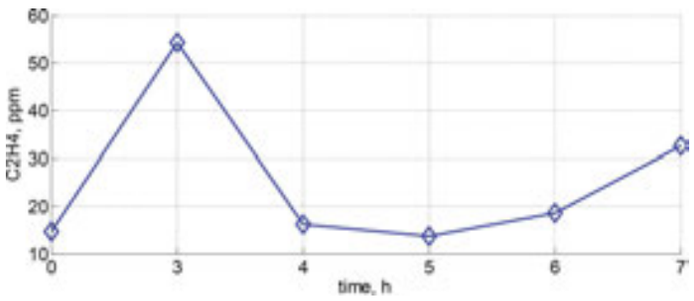

Figure 91. C2H4.

The breakdown voltage "Up" increases with time of PD generation. Similar relationship was observed for the following parameters: H2, N2, CH4 and C2H2. The water content decreases with the PD generation time. There is no significant influence of the PD generation time on the following parameters: O2, TCG, CO, CO2, C3H6, C3H8, C2H6, C2H4.

4. Conclusions

When considering the electrical and UHF methods, one can state the following conclusions:

- The most significant frequencies which were selected based on the UHF amplitude spectra are similar for all three electrodes arrangements.
- For data gathered in the NN and SURF systems, the empirical distribution of charges, registered with the electrical method, depicted no significant differences between the three considered frequency values. In the case of voltages, registered with the UHF method, the densities are different for the particular frequency ranges.
- For data gathered in the NNB system, it was observed that all charts, depicting empirical distributions of data gathered with the electric and UHF methods, are normally distributed independently of the phase of the supply voltage.

When considering the spectrophotometry method, the following conclusions can be stated:

http://dx.doi.org/10.5772/62409

- Analysis of the optical spectra, registered during PD generation at different voltage levels and distances in the NN and NNB systems, resulted with the statement that there is no significant influence of the voltage value at the registered intensities. This was confirmed by presentation of the maximal intensities, determined from the registered spectra, in the function of PD generation voltage. The lacking dependency was also confirmed by determining the energy of the registered optical spectra. For both NN and NNB systems, there was recognized no significant dependency of the voltage value on the energy contained in the spectra regardless of the distance at which the measuring sensor was installed.
- Analysis of the optical spectra, registered during PD generation at different voltage levels and distances in the SURF system, resulted with the statement that there is a clear dependency of voltage on the registered intensity spectra, which was farther depicted by presentation of the maximal intensities and energy values in the function of PD generation voltage.

When considering the acoustic emission, the conclusion was stated that there is no significant influence of PD generation voltage on the frequency components included in the PSD spectra, which were previously calculated for the AE signals registered in the NN and SURF system.

Analysis of UV and MIR images resulted with the statement that the is no such radiation apparent outside the tank. The same regards to high energy signals.

The most important conclusions related to the chromatography method are the following: the breakdown voltage Up and the H2, N2, CH4 and C2H2 values increase with the time of PD generation. Only the water content decreases with the PD generation time. The other parameters are not influenced by the PD generation time.

5. Summary

The main cognitive-scientific aim of the project is a detailed and multi-variate research study of physical phenomena associated with the generation of basic types of PD, which occur in the electro-insulation oil.

Based on the current knowledge, implied on literature reviews carried out by the authors as part of previous works and technical expertise, regarding the considered subject matter, it was stated that until now systematic research aimed to understanding of the phenomenon of PD generation in insulation oil has not been performed, which would include analyses of all physical phenomena simultaneously, i.e., under identical measurement conditions. In addition, no assessment was made of their interrelationships.

The experimental works performed within the research tasks involved measurement of acoustic emission and electrical signals, high-frequency electromagnetic and high-energy (X-rays/gamma) radiation, optical and thermal images, which are the common phenomena generated by PD. Three systems were designed and built for modelling of different types of PD: a surface system, a needle-needle system and a needle-needle system with gas bubbles. In the final effect, the most effective methods of PD measurement and evaluation were selected.

The research hypothesis that it is possible to investigate experimentally the physical processes related to generation of basic PD forms which can occur in insulation oil, was confirmed.

It should be emphasized that the objective and multivariate investigation of the PD phenomenon is an extremely important issue, not only from the cognitive point of view but also has an utilitarian value. This relates to application of the obtained dependencies for correlation of achieved results and by this means for improvement of the diagnostic methods applied for evaluation of high-voltage insulating systems of power transformers, which are essential in the system of arranging the distribution and transmission of electricity. Thus, the results obtained may have a measurable trade and industrial importance, having a direct impact on economic and financial aspects, and indirectly to the development of civilization, and a very strong social aspect.

Acknowledgements

The work was co-financed from funds of the National Science Centre (NCS) as part of the OPUS programme, project no.: 2013/09/B/ST8/01736.

The work was co-financed by the European Regional Development Fund "Increase of Scientific Research and Innovation for Enterprises in Terms of Sustainable Development Through the Creation of a Modern Diagnostics Laboratory of Surge Voltage" at the Opole University of Technology – Part I (2010–2011) and Part II (2011–2013), Project no RPO. 01.03.0101-16-007/10-00 and WND-RPOP.01.03.01-16-007/10.

Author details

Tomasz Boczar, Andrzej Cichoń, Daria Wotzka*, Paweł Frącz, Michał Kozioł and Michał Kunicki

*Address all correspondence to: daria@wotzka.eu

Opole University of Technology, Opole, Poland

References

[1] Jacob N.D. ; McDermid W.M. ; Kordi B.: On-line monitoring of partial discharges in a HVDC station environment, IEEE Transactions on Dielectrics and Electrical Insulation, Vol. 19, no 3, 2012, pp. 925 – 935

http://dx.doi.org/10.5772/62409

[2] Cavallini A. ; Montanari G.C. ; Tozzi M. ; Chen, Xiaolin: Diagnostic of HVDC systems using partial discharges, IEEE Transactions on Dielectrics and Electrical Insulation, Vol. 18, no 1, 2011, pp. 275 – 284

[3] Pompili M. ; Bartnikas R.: On partial discharge measurement in dielectric liquids, IEEE Transactions on Dielectrics and Electrical Insulation, Vol. 19, no 5, 2012, pp. 1476 – 1481

[4] Lindell E. ; Bengtsson T. ; Blennow J. ; Gubanski S.M.: Evaluation of a PD measuring system for repetitive steep voltage waveforms, IEEE Transactions on Dielectrics and Electrical Insulation, Vol. 18, no 1, 2011, pp. 246 – 255

[5] El-Hag A.H. ; Saker Y.A. ; Shurrab I.Y.: Online Oil Condition Monitoring Using a Partial- Discharge Signal, IEEE Transactions on Power Delivery, Vol. 26, no 2, 2011, pp. 1288 – 1289

[6] Lopatkiewicz R. ; Nadolny Z. ; Przybylek P.: The Influence of Water Content on Thermal Conductivity of Paper Used as Transformer Windings Insulation, 10th IEEE International Conference on the Properties and Applications of Dielectric Materials (ICPADM), JUL 24–28, 2012, India.

[7] Montanari G.C. ; Cavallini A.: Partial discharge diagnostics: from apparatus monitoring to smart grid assessment, IEEE Electrical Insulation Magazine, Vol. 29, no 3, 2013, pp. 8 – 17

[8] Junhao L. ; Quanwei H. ; Xuefeng Z. ; Xiu Y. ; Yongfen Y. ; Yanming Y.: Partial-Discharge Characteristics of Free Spherical Conducting Particles Under AC Condition in Transformer Oils, IEEE Transactions on Power Delivery, Vol. 26, no 2, 2011, pp. 538 – 546

[9] Yoshida M. ; Kojima H. ; Hayakawa N. ; Endo F. ; Okubo H.: Evaluation of UHF method for partial discharge measurement by simultaneous observation of UHF signal and current pulse waveforms, IEEE Transactions on Dielectrics and Electrical Insulation, Vol. 18, no 2, 2011, pp. 425 – 431

[10] Rodrigo A. ; Llovera P. ; Fuster V. ; Quijano A.: Influence of high frequency current transformers bandwidth on charge evaluation in partial discharge measurements, IEEE Transactions on Dielectrics and Electrical Insulation, Vol. 18, no 5, 2011, pp. 1798 – 1802

[11] Reid A.J. ; Judd M.D. ; Fouracre R.A. ; Stewart B.G. ; Hepburn D.M.: Simultaneous measurement of partial discharges using IEC60270 and radio-frequency techniques, IEEE Transactions on Dielectrics and Electrical Insulation, Vol. 18, no 2, 2011, pp. 444 – 455

[12] Jian L. ; Tianyan J. ; Harrison R.F. ; Grzybowski S.: Recognition of ultra high frequency partial discharge signals using multi-scale features, IEEE Transactions on Dielectrics and Electrical Insulation, Vol. 19, no 4, 2012, pp. 1412 – 1420

[13] Robles G. ; Sanchez-Fernandez M. ; Albarracin Sanchez R. ; Rojas-Moreno M.V. ; Rajo-Iglesias E. ; Martinez-Tarifa J.M.: Antenna Parametrization for the Detection of Partial Discharges, IEEE Transactions on Instrumentation and Measurement, Vol. 62, 932 – 941

[14] Boczar T. ; Zmarzly D.: The application of correlation analysis to acoustic emission pulses generated by partial discharges, Materials Evaluation, Vol. 62, pp. 2004, 935 – 942, 2004

[15] Wotzka D. ; CichońA. Boczar T.: Modeling and Experimental Verification of Ultrasound Transmission in Electro Insulation Oil, Archives of Acoustics, Vol. 37, no. 1, 2012, pp. 19 – 22

[16] Szmechta M. ; Boczar T. ; Frącz P.: Frequency and Time-Frequency Analysis of Acoustic Cavitation Noise in Insulating Oils, Acta Physicsa Polonica A, Vol. 120, 2011, pp. 744 – 747

[17] Borucki S. ; CichońA.: The influence of the power transformer load on vibroacoustic signal analysis results, Przegląd Elektrotechniczny Vol. 86, 2010, pp. 45 – 47

[18] Borucki S. ; Boczar T. ; Cichon A.: Investigation of the acoustic pressure distribution occurring around an aerial substation adjacent to apartment buildings, Archives of Acoustics, Vol.32, No. 4, 2007, pp. 291 – 297

[19] CichońA. ; Borucki S. ; Wotzka D. ; Szmajda M.: Characteristic of acoustic emission signals generated by the contacts of the selector, Acta Physica Polonica A, Vol. 122, Issue 5, 2012, pp. 804 – 807

[20] Wotzka D. ; Zmarzly D. ; Boczar T.: Numerical simulation of acoustic wave propagating in a spherical object filled with insulating oil, Acta Physica Polonica A, Vol. 118, Issue 6, 2010, pp. 1272 – 1275

[21] Fracz P. ; Boczar T. ; Zmarzly D. ; et al.: Analysis of optical radiation generated by electrical discharges on support insulator, Acta Physica Polonica A, Vol. 124, Issue 3, 2013, pp. 413 – 416

[22] Fracz P. ; Boczar T. ; Borucki S. ; CichońA. ; Zmarzly D.: Results of optical signals analyses emitted by electrical discharges recorded with UV camera, Acta Physica Polonica A, Vol. 122, Issue 5, 2012, pp. 814 – 817

[23] Fracz P. ; Zmarzly D. ; Boczar T.: Characteristic of surface partial discharges measured with ultraviolet camera, Acta Physica Polonica A, Vol. 127, Issue 3, 2015, pp. 715 – 718

[24] Zmarzły D. ; Nagi L. ; Borucki S. ; Boczar T.: Analysis of ionizing radiation generated by partial discharges, Acta Physica Polonica A, Vol. 125, Issue 6, 2014, pp. 1377 – 1379

[25] Zmarzły D. ; Nagi L. ; Frącz P. ; Boczar T.: Detection of high-energy ionizing radiation generated by electrical discharges in oil, IEEE Transactions on DEIS, 2016, accepted for publication

[26] Boczar T. ; Cichoń S. Kunicki M. ; Kozioł M. Wotzka D.: Indicator Analysis of Partial Discharges Measured Using Various Methods in Paper-Oil Insulation, IEEE Transactions on DEIS, 2016, under review.